

Article

# Multimineral Fingerprinting of Transhimalayan and Himalayan Sources of Indus-Derived Thal Desert Sand (Central Pakistan)

Wendong Liang \*, Eduardo Garzanti \* , Sergio Andò, Paolo Gentile and Alberto Resentini

Laboratory for Provenance Studies, Department of Earth and Environmental Sciences, University of Milano-Bicocca, Piazza della Scienza 4, 20126 Milano, Italy

\* Correspondence: w.liang@campus.unimib.it (W.L.); eduardo.garzanti@unimib.it (E.G.)

Received: 16 July 2019; Accepted: 24 July 2019; Published: 26 July 2019



**Abstract:** As a Quaternary repository of wind-reworked Indus River sand at the entry point in the Himalayan foreland basin, the Thal Desert in northern Pakistan stores mineralogical information useful to trace erosion patterns across the western Himalayan syntaxis and the adjacent orogenic segments that fed detritus into the Indus delta and huge deep-sea fan throughout the Neogene. Provenance analysis of Thal Desert sand was carried out by applying optical and semi-automated Raman spectroscopy on heavy-mineral suites of four eolian and 11 fluvial sand samples collected in selected tributaries draining one specific tectonic domain each in the upper Indus catchment. In each sample, the different types of amphibole, garnet, epidote and pyroxene grains—the four dominant heavy-mineral species in orogenic sediment worldwide—were characterized by SEM-EDS spectroscopy. The chemical composition of 4249 grains was thus determined. Heavy-mineral concentration, the relative proportion of heavy-mineral species, and their minerochemical fingerprints indicate that the Kohistan arc has played the principal role as a source, especially of pyroxene and epidote. Within the western Himalayan syntaxis undergoing rapid exhumation, the Southern Karakorum belt drained by the Hispar River and the Nanga Parbat massif were revealed as important sources of garnet, amphibole, and possibly epidote. Sediment supply from the Greater Himalaya, Lesser Himalaya, and Subhimalaya is dominant only for Punjab tributaries that join the Indus River downstream and do not contribute sand to the Thal Desert. The detailed compositional fingerprint of Thal Desert sand, if contrasted with that of lower course tributaries exclusively draining the Himalaya, provides a semi-actualistic key to be used, in conjunction with complementary provenance datasets and geological information, to reconstruct changes in paleodrainage and unravel the relationship between climatic and tectonic forces that controlled the erosional evolution of the western Himalayan-Karakorum orogen in space and time.

**Keywords:** amphibole; garnet; epidote; pyroxene; provenance tracers; varietal studies; mineral chemistry; semi-automated Raman counting; Ladakh-Kohistan arcs; Himalaya; Nanga Parbat; Karakorum; Indus river

## 1. Introduction

Heavy minerals provide detailed information on the geology of source areas, which is particularly useful in the study of modern sand unmodified by diagenesis [1]. Subtler distinctions, however, may be required in provenance analysis wherever several different potential sources of sediment consist of similar lithological assemblages shedding similar heavy-mineral assemblages. This is often the case in orogenic sediment containing transparent-heavy-mineral suites typically dominated by amphibole, garnet, epidote, and pyroxene in various proportions [2–4]. In this case, distinctive geochemical signatures of single groups of detrital minerals can be used as a genetic tool to trace their provenance (“varietal studies”; [5]).

After the pioneering study dedicated to tourmaline by Krynine [6], and since modern geochemical techniques were applied on garnet [7], single-mineral analyses have been frequently used and proven to be an efficient means to trace sediment provenance (e.g., [8–12]). More and more sophisticated geochemical and geochronological methods are being applied with the aim to fingerprint the source of an increasing number of target minerals (e.g., [13]). Single-mineral studies have the advantage that fractionation by physical processes during erosion, transport and deposition, and by chemical processes during weathering and diagenesis, can generally be held as minimal. On the other hand, the information obtained from single-mineral datasets needs to be deciphered by correcting for the generally strong differences in mineral fertility of different potential source rocks [14,15]. This thorny fertility problem is best tackled when several mineral groups are investigated (“multimineral fingerprinting”; [16,17]), because provenance signals carried by different minerals are expected to differ, reflecting their different abundance in different source-rock domains. Emphasizing this crucial point is one of the goals of this article, which focuses on Transhimalayan and Himalayan sources of detritus transported by the Indus River across northern Pakistan to pinpoint the provenance of heavy minerals contained in eolian sand of the Thal Desert. This small dune field is located in central-northern Pakistan, confined between the Indus River in the west and the course of its major Punjab tributaries in the east (Figure 1). The overall petrographic, mineralogical, and geochemical signatures of Thal dunes indicate that the contribution of Himalayan-derived Punjab tributaries is negligible [18]. The Thal Desert, therefore, can be safely considered as representing a relict Quaternary repository of wind-reworked alluvial-fan sediment originally deposited by the upper Indus at the entry point in the Himalayan foreland basin. The detailed compositional fingerprint of Thal Desert sand, if contrasted with that of Punjab tributaries exclusively draining the Himalayan belt, thus provides an additional actualistic key to trace changes in erosion patterns within the huge catchment that has fed detritus to the Indus delta and deep-sea fan throughout the late Neogene [19,20]. To this goal, our dataset complements a previous work on major and trace elements in amphibole [21] and integrates the geochemical study of detrital garnet in sand of the middle Indus course and its Punjab tributaries [22]. We chose to focus on the chemical composition of detrital amphibole, garnet, epidote, and pyroxene because these four minerals, all solid-solution series, represent the four dominant species in orogenic sediments worldwide [23]. Other studies investigating provenance of Indus sediments focused on Pb isotopes in detrital K-feldspar and bulk-sediment Nd and Sr isotope fingerprints [24–26], zircon U-Pb or mica  $^{39}\text{Ar}/^{40}\text{Ar}$  geochronology and apatite fission-track or (U–Th)/He thermochronology [27–29], sand petrography, heavy minerals,  $^{10}\text{Be}$  cosmogenic nuclides [18,30], and clay mineralogy [31]. Such multi-technique approaches have shed new light on the relative role played by the interacting climatic and tectonic forces that controlled the erosional evolution of the western Himalayan-Karakorum orogen.

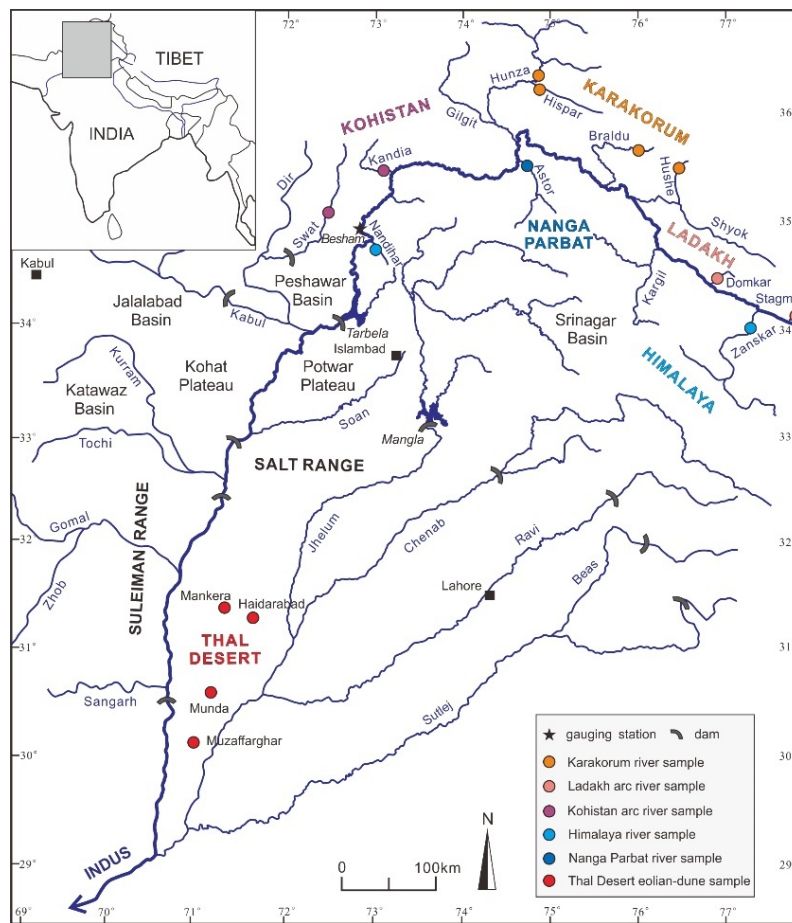


Figure 1. The Indus drainage system and sample locations in northern Pakistan.

## 2. The Indus River Catchment and the Thal Desert

The Indus River, sourced from the central southern Tibetan Plateau, flows in its upper course along the suture zone and Transhimalayan forearc basin, while receiving detritus from both the Ladakh arc in the north and the northern side of the Himalayan belt in the south [30]. Next, it cuts a deep gorge through the western Himalayan syntaxis, where very rapid erosion rates generate large amounts of detritus from the Karakorum belt, the Nanga Parbat crystalline massif, and the Kohistan arc [32–35]. Farther downstream, it flows across the Himalayan belt and Potwar Plateau [36] where it is joined by the Kabul River draining the Hindukush belt [37], crosses the Salt Range, and eventually reaches the foreland basin where it flows southward, confined between the front of the Sulaiman Range in the west and the Thal Desert in the east (Figure 1).

The upper Indus River is mainly fed by melting of ice and snow, and sediment flux consequently increases by two to three orders of magnitudes during the summer [38]. The annual suspended load of the Indus River, estimated as  $\sim 14 \times 10^6$  t upstream of the Shyok confluence (Figure 1), increases rapidly downstream owing to major contributions from the Shyok River ( $\sim 23 \times 10^6$  t/a), Karakorum tributaries ( $\leq 100 \times 10^6$  t,  $\sim 18 \times 10^6$  of which from the Hunza River), the Astor River draining Nanga Parbat ( $\sim 2 \times 10^6$  t), and diverse tributaries draining the Kohistan arc, summing up to  $\sim 176 \times 10^6$  t at the Besham gauging station [39]. The annual sediment load reaching the Tarbela Dam, which was closed in 1974 in northern Pakistan, has been estimated at  $200 \times 10^6$  t [40,41] or even at  $287 \times 10^6$  t [42].

The hydrology of the Indus River has been so intensely regulated since the 1930s that most of its sediment has been trapped in artificial reservoirs and canals, and the annual flux in the lower course has been reduced to  $\sim 50 \times 10^6$  t [42]. The Indus Waters Treaty signed in 1960 gave rights to the entire flow of the Indus, Jhelum, and Chenab Rivers to Pakistan, and of the Ravi, Beas, and Sutlej Rivers to India.

Subsequently, all Punjab tributaries have been dammed and linked by canals to irrigate the arid lowlands and compensate for lost waters in eastern Pakistan. Water discharge dropped sharply, and flow in the Ravi and Sutlej rivers ceased altogether except during monsoon floods. The Mangla Dam, completed in 1967, reduced sediment load of the Jhelum River from 45 to  $< 0.5 \times 10^6$  t/a [43,44]. Among Indus tributaries draining the Sulaiman Range in western Pakistan, the Gomal River (basin area 36,000 km<sup>2</sup>) is characterized by extreme concentration of suspended solids (42 g/L) and high sediment load ( $30 \times 10^6$  t/a), followed by the Kurram River ( $3 \times 10^6$  t/a; [42]). Other rivers are minor and mostly flow during flash floods.

### 2.1. Karakorum Belt

The composite Karakorum belt includes the Northern Karakorum sedimentary domain, the Central Karakorum batholith, and the Southern Karakorum metamorphic belt (Figure 2; [45,46]). In the Northern Karakorum zone, an Ordovician to Upper Cretaceous sedimentary succession lying non-conformably onto crystalline basement is exposed [47]. Black slates in the north, intruded by calc-alkaline gabbro-diorite, granodiorite, granite, and tonalite, contain andalusite, chloritoid, and epidote [48]. The Central Karakorum batholith comprises mid-Cretaceous granitoids intruded before the India-Asia collision and containing amphibole with residual clinopyroxene and accessory titanite, epidote, allanite, apatite, zircon, and opaque minerals [49]. Post-collisional leucogranites were intruded between 13 and 25 Ma (e.g., Baltoro batholith; [50]). The Southern Karakorum belt includes migmatitic domes undergoing rapid erosional exhumation and displays a northeastward increase in metamorphic grade from structurally lower phyllites to staurolite-, kyanite-, and eventually sillimanite-bearing metasedimentary rocks at the top. Impure dolomitic marbles containing diopside and corundum, and amphibolites with hornblende and garnet also occur [51–53].

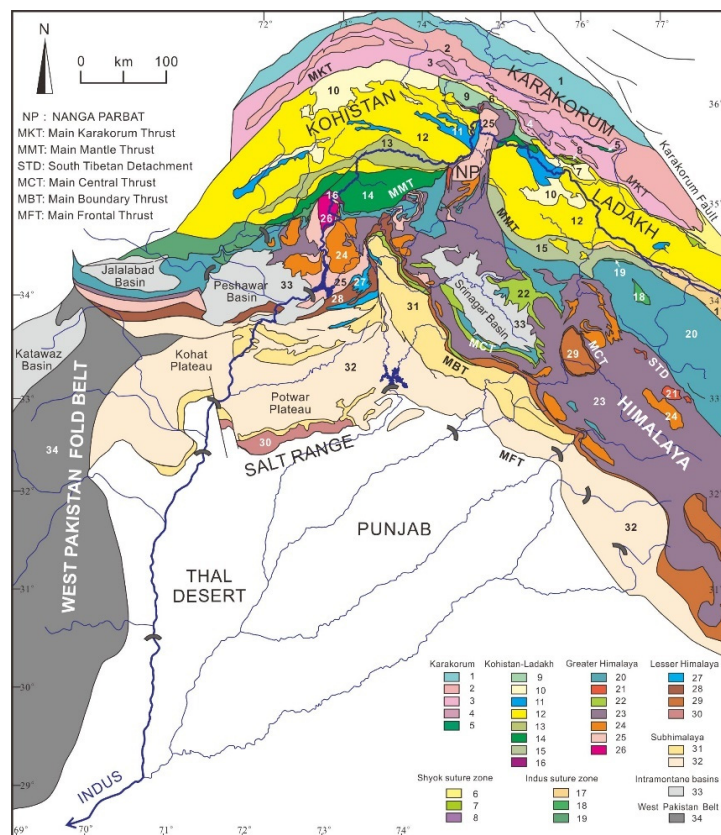


**Figure 2.** Geological map of the Indus catchment in northern Pakistan (modified from Pêcher et al. [34]). Geological units, from north to south: **Karakorum belt:** 1: northern sedimentary belt; 2: axial batholith and other granitoid rocks; 3: southern metamorphic belt; 4: felsic gneiss; 5: Masherbrum Greenstone Complex. **Shyok suture zone:** 6: mostly terrigenous strata; 7: mélangé zone (mainly volcanic rocks);

8: ultramafic rocks (Shyok and Dobani-Dassu lineament). **Kohistan and Ladakh arcs:** 9: Paleogene Chalt (Kohistan) and Khardung (Ladakh) volcanic rocks, Turmik volcanoclastic rocks; 10: undifferentiated volcano-sedimentary group; 11: metasedimentary rocks; 12: plutonic rocks; 13: gabbro-norite (Chilas complex); 14: southern amphibolite; 15: Dras volcano-sedimentary group; 16: ultramafic rocks (Jijal complex). **Indus suture zone:** 17: Indus Group; 18: Spontang ophiolite; 19: imbricate thrust units with blueschist. **Tethys and Greater Himalaya:** 20: Paleozoic-Eocene sedimentary rocks; 21: Miocene leucogranite; 22: Permian Panjal Traps; 23: Greater Himalayan neometamorphic rocks; 24: Paleozoic intrusives; 25: mainly Paleoproterozoic orthogneiss; 26: Besham metaigneous rocks. **Lesser Himalaya:** 27: Paleozoic-Eocene strata; 28: upper nappe (mostly Mesoproterozoic metasedimentary rocks); 29: lower nappe (mostly Neoproterozoic and Paleozoic metasedimentary rocks); 30: Salt Range (Neoproterozoic to Eocene Indian margin strata). **Sub-Himalaya:** 31: Muree and Subathu formations (Cenozoic); 32: Siwalik Group (Neogene); 33: Peshawar and Srinagar Quaternary intramontane basins. **West Pakistan Belt:** 34: Sulaiman Range.

## 2.2. Ladakh and Kohistan Arcs

The Ladakh and Kohistan batholiths expose a complete section of mantle to upper crustal igneous rocks representing the dissected remnants of magmatic arcs fed by northern subduction of Neotethyan lithosphere during the Cretaceous to earliest Paleogene. The arcs are delimited by the Shyok ophiolitic suture in the north, generally ascribed to Upper Cretaceous (pre-Campanian) collision with the Karakorum block [54–58], and the Indus ophiolitic suture in the south, closed when India collided with Asia during the Paleocene [59,60].

The Kohistan arc is composed of six main units from bottom to top (south to north): (1) Jijal ultramafic-mafic complex yielding garnet, amphibole, clinopyroxene, and minor olivine, orthopyroxene, spinel and zoisite; (2) Kamila amphibolite; (3) Chilas ultramafic-mafic complex, containing orthopyroxene and clinopyroxene with minor olivine, magnetite, ilmenite, hornblende, and spinel; (4) Kohistan batholith, yielding mainly hornblende and locally clinopyroxene; (5) Jurassic-Cretaceous metavolcanic and metasedimentary rocks of the Jaglot and Chalt Groups, and the Aptian-Albian volcano-sedimentary Yasin Group [61–63].

The Ladakh batholith consists of a suite of Cretaceous to Paleogene mafic to felsic rocks (olivine norite to granite) yielding hornblende, augite, titanite, apatite, epidote, and zircon [64,65]. The batholith is non-conformably overlain by Upper Cretaceous to Paleogene strata of the Indus Group [66,67]. Rocks exposed along the Indus suture also include Lower Cretaceous carbonates, ophiolitic mélange, and blueschists [68,69].

## 2.3. Himalayan Belt and Nanga Parbat Massif

The Himalayan Range formed as a consequence of continental collision between the Indian passive margin and the Asian active margin at ~60 Ma [70,71]. The orogenic belt consists of a series of southward propagating thrust sheets, which resulted in crustal thickening starting from the Eocene [72,73]. The Neoproterozoic to Eocene Tethys Himalayan succession consists of siliciclastic and carbonate rocks originally deposited onto the northern continental margin of India [74,75]. The Greater Himalaya, including slate intruded by Ordovician granitoids and sillimanite-bearing metasedimentary rocks at the top, represents the axial crystalline backbone of the range [33,76]. It is delimited in the north by the South Tibetan Detachment system lined with Miocene tourmaline-bearing leucogranite intrusions [77] and by the Main Central Thrust in the south [78]. Lesser Himalayan and Sub-Himalayan rocks exposed farther south include, respectively, Paleoproterozoic basement and Mesoproterozoic to Cenozoic cover strata displaying southward decreasing metamorphic grade [79,80] and orogen-derived Cenozoic molasse [81–83]. These rocks are drained by Punjab tributaries and shed detritus that contributes to Indus River load only downstream of the Thal Desert.

Only the Indus River cuts across the western Himalayan syntaxis, where the N/S-elongated crustal-scale Nanga Parbat antiform exposing Precambrian Indian gneissic basement overprinted by Himalayan metamorphism is bounded to the north by the Karakorum belt and flanked to the west and

east by the Kohistan and Ladakh arcs. In the Nanga Parbat massif, sillimanite-bearing gneisses are structurally overlain by kyanite-bearing schists [84,85]. Leucogranite intrusions yielding tourmaline, apatite, zircon, monazite, and garnet [86] are as young as 1.4 Ma. Cooling ages of 5 Ma or even 1 Ma in the core of the dome [87] testify to ultra-rapid exhumation and very fast fluvial incision [88,89], with high denudation rates of 3–5 mm/year [90–92]. Upstream of the entry point in the foreland basin, the Indus River traverses the Potwar Plateau, where Himalayan-derived molassic Cenozoic rocks are widely exposed [93,94], and finally cuts across the Salt Range, including Paleozoic to Paleogene strata detached over uppermost Neoproterozoic/Cambrian salt and uplifted during the latest Miocene [95].

#### 2.4. Thal Desert

The Thal Desert, a triangular region located in central northern Pakistan between  $\sim 30^\circ$  and  $32^\circ 30'$  N and between  $\sim 71^\circ$  and  $72^\circ$  E (Figure 2), is characterized by arid to semi-arid subtropical climate. This desert occupies the Sind-Sagar or Thal Doab (*doab* = land between two rivers, from *do* = two and *ab* = water in Urdu and Farsi), the region extending between the course of the Indus River in the west and the Punjab in the east, the fertile region crossed by the Himalayan rivers Jhelum, Chenab, Ravi, Beas, and Sutlej (*punjab* = five waters, from *panj* = five and *ab* = water).

The Thal Desert is delimited by the Salt Range foothills in the north, whereas the Indus floodplain is bounded by the Sulaiman Range in the west (Figure 1). The desert area is covered by low sand dunes (1–2 m in height) or rolling sand plains alternating with narrow valleys of cultivable land, and is underlain by Quaternary fluvial and eolian deposits more than 350 m thick in the south and even thicker in the central part of the desert [96]. The underlying alluvium mostly consists of laterally continuous fine to coarse sand, with minor gravel and isolated mud lenses. The coarsest deposits occur in the north close to the Salt Range, but otherwise the distribution of grain size is irregular, reflecting deposition by the constantly shifting paleo-Indus River.

### 3. Methods

#### 3.1. Sampling

The sample set considered in this study includes four eolian-dune sand samples collected in February 2001 from the Thal Desert, along with 11 sand samples collected during 2001 and 2011 from active river bars in 11 tributaries draining each a different geological domain in the upper Indus River catchment (“first-order sampling scale” of [97]). These samples were accurately selected from a much larger sample set, described elsewhere [18,30,98], as the best suited to represent end-member sources of detritus derived from the Karakorum belt (upper Hushe, upper Braldu, upper Hunza, and Hispar samples), the Ladakh (Stagmo and Domkar samples) and Kohistan arcs (Kandia and Swat samples), the Nanga Parbat massif (Astor sample), and the Himalayan belt (Zaskar and Nandihar samples). The Thal dune samples are upper very fine to lower fine and well to moderately sorted sands ( $3.05\text{--}2.67 \Phi$ ,  $0.43\text{--}0.84 \sigma_\Phi$ ); fluvial samples are upper very fine to lower medium and moderately-well to moderately sorted sands ( $3.20\text{--}1.51 \Phi$ ,  $0.63\text{--}0.97 \sigma_\Phi$ ) (Supplementary Table S1).

#### 3.2. Heavy Mineral Analyses

For each of the 15 selected samples, heavy minerals were separated with sodium polytungstate (density  $\sim 2.90 \text{ g/cm}^3$ ) from a split aliquot of the 63–250  $\mu\text{m}$  or 32–500  $\mu\text{m}$  fraction obtained by sieving, recovered by partial freezing with liquid nitrogen, and mounted on a glass slide. A polished thin section was also prepared, and mineralogical composition was determined by both counting under the microscope of  $\geq 200$  transparent heavy minerals in the glass slide and by semi-automated analysis of the polished thin section with a Raman spectrometer [99].

Heavy-mineral concentration, calculated as the volume percentage of total (HMC) and transparent (tHMC) heavy minerals in the bulk sample, ranges from poor (tHMC  $< 1$ ), moderately poor

( $1 \leq \text{tHMC} < 2$ ) and moderately rich ( $2 \leq \text{tHMC} < 5$ ), to rich ( $5 \leq \text{tHMC} < 10$ ), very rich ( $10 \leq \text{tHMC} < 20$ ) and extremely rich ( $20 \leq \text{tHMC} < 50$ ) [100,101].

### 3.3. Sources of Bias

As a consequence of choosing a  $2\Phi$  to  $4\Phi$ -wide size window for analysis in order to reduce technical problems during separation, mounting on the glass slide and identification under the microscope caused by detrital grains with great size differences, heavy minerals occurring in the finest tail of the size distribution ( $3\% \pm 2\%$  of each bulk sample) and in the coarse tail ( $32\% \pm 22\%$  of each bulk sample) were discarded. The sediment fraction considered for analysis ranged between  $58\% \pm 21\%$  for fluvial samples to  $85\% \pm 9\%$  for the better sorted Thal eolian-dune samples. The analytical bias thus introduced can be considered as minor, because the fine tail was almost entirely included whereas the coarse tail is strongly depleted in heavy minerals as the concentration of denser grains drops rapidly in the coarser classes of sediments deposited by tractive currents [102,103].

Another potential source of bias is represented by hydraulic-sorting processes, which may concentrate different minerals in distinct depositional sub-environments based on their size, density, and shape [104–106]. An efficient way to test for heavy-mineral enrichment or depletion in sediment samples is provided by chemical analyses, which readily reveal anomalous concentrations of chemical elements such as rare earth elements (REE) or zirconium preferentially hosted in ultradense minerals [101]. Among the four Thal dune samples, heavy-mineral enrichment is apparent for the Muzaffargarh sample S1470 containing much more Zr than the Munda sample S1474 (524 vs. 106 ppm), whereas the other two samples S1462 and S1463 have Zr concentration very close to the Upper Continental Crust standard (UCC; 195–213 vs. 190–193 ppm in the UCC; [107,108]) (Supplementary Table S1). Among river sands, only the Hispar sample shows high concentration of Zr, Th, and REEs relative to all other samples (Zr 395 vs. 110–186 ppm; Th 52 vs. 3–14 ppm; La 117 vs. 12–55 ppm and Y 41 vs. 12–27 ppm), suggesting hydraulic enrichment in heavy minerals. The heavy-mineral spectrum of samples systematically showing anomalous concentrations in these elements is expected to be enriched in denser heavy minerals such as garnet relative to low-density heavy minerals such as amphibole.

### 3.4. Microchemical Analyses

The same polished thin sections, in a photographic image of which all grains were properly identified and numbered, were carbon-coated and analyzed by Energy Dispersive X-ray Spectroscopy (EDS) under the scanning electron microscope (SEM) to obtain quantitative chemical information on the four most common detrital minerals in orogenic sediments (i.e., amphibole, garnet, epidote, and pyroxene). Microchemical analyses were carried out at the Department of Earth and Environmental Sciences, University of Milano-Bicocca (Milano, Italy), using a TESCAN TS5136XM with an electronic microprobe EDAX GENESIS 4000 XMS Imaging 60 SEM, voltage 20 KeV, detection time 20 s, spot size 250 nm and absorption current  $190 \pm 1$  pA measured in Faraday cup, medium heating, take off angle  $45^\circ$ , working distance 23 mm. In each thin section, we counted  $\sim 100$  grains for each mineral group (or all of those present in case we did not find enough). In the four Thal Desert samples, 400 amphibole, 395 epidote, 317 pyroxene, and 280 garnet grains were analyzed, thus allowing identification even of small detrital populations [109]. Overall, we analyzed 1504 amphibole, 1129 epidote, 861 pyroxene, and 755 garnet grains in the 15 selected samples. Information on sample locations, the result of heavy-mineral analyses, and the complete geochemical dataset including the percentages of each mineral variety in each sample are provided as Supplementary Material (Tables S1–S10). Statistical techniques used to illustrate our dataset include multidimensional scaling, which produces a map of points in which samples with similar mineralogical signature cluster closely together and dissimilar samples plot far apart [110] and the biplot [111], which allows us not only to discriminate among multivariate observations (data points) but also to visualize the mutual relationships among an even large number of variables (rays). The length of each ray is proportional to the variance of the corresponding parameter

in the dataset, whereas if the angle between two rays is close to 0°, 90° or 180°, then the corresponding elements are directly correlated, uncorrelated or inversely correlated, respectively.

### 3.5. Amphibole Chemistry

The general chemical formula of the amphibole supergroup is  $AB_2C_5T_8O_{22}W_2$ , where A, B, and C are cations and W anions (A = □, Na, K, Ca, Pb, Li; B = Na, Ca,  $Mn^{2+}$ ,  $Fe^{2+}$ , Mg, Li; C = Mg,  $Fe^{2+}$ ,  $Mn^{2+}$ , Al,  $Fe^{3+}$ ,  $Mn^{3+}$ ,  $Ti^{4+}$ ,  $V^{3+}$ , Li; T = Si, Al,  $Ti^{4+}$ , Be; W = (OH), F, Cl,  $O^{2-}$ ; [112,113]). Following the recommendation of the International Mineralogical Association, amphibole minerals are divided into two groups based on the dominant anions at site W, i.e., (OH, F, Cl)<sup>−</sup> versus oxo-amphiboles. The (OH, F, Cl)<sup>−</sup> group is further subdivided into eight subgroups based on B cations. An Excel spreadsheet developed by Locock [114] was used to calculate the chemical formula and classify detrital amphiboles. The  $Fe^{3+}/\Sigma Fe$  and  $Mn^{3+}/\Sigma Mn$  ratios were calculated based on charge balance by normalizing the formula to one or more sets of cation sums because the valence state of Fe and Mn was not measured. All amphibole grains were considered to be monoclinic because only a few (<2%) orthorhombic amphibole grains were detected with Raman spectroscopy. For amphibole with W = 2 (OH, F, Cl), sufficient OH content was calculated to reach two (OH, F, Cl) per formula unit because  $H_2O^+$  was not measured and OH could not be estimated [114].

### 3.6. Garnet Chemistry

The general formula of garnet contains eight cations and 12 anions:  $X_3Y_2Z_3\Phi_{12}$ , where X = Na, Mg, Ca,  $Mn^{2+}$ ,  $Fe^{2+}$ , Y; Y = Mg, Al, Si, Sc, Ti, V, Cr,  $Mn^{3+}$ ,  $Fe^{2+}$ ,  $Fe^{3+}$ , Zr, Sn; Z = Al, Si,  $Fe^3$ . The Excel spreadsheet developed by Locock [115], which considers 15 different garnet varieties and 14 end-members was used to calculate the molar proportion of garnet end-members from chemical data. The iron was entered as  $FeO_{tot}$  in the spreadsheet and the amounts of  $Fe^{2+}$  and  $Fe^{3+}$  were calculated by stoichiometric constraints because the proportion of FeO vs.  $Fe_2O_3$  was not determined.  $Mn^{3+}$  was calculated only for compositions that cannot charge balance with  $Fe^{3+}$  alone.

Garnet, common in orogenic sediments derived from metasedimentary rocks, is a particularly valuable provenance tracer because it displays a wide range of major-element compositions and resists diagenetic dissolution better than epidote, amphibole, and pyroxene [116–118].

Different types of detrital garnets can be empirically distinguished according to their provenance by the use of the Fe + Mn–Mg–Ca ternary plot [5,119]. Type A garnet (high Mg, low Ca) is mainly shed by granulite-facies metasedimentary rocks, charnockites, and intermediate-felsic igneous rocks. Type B garnet (low Mg, variable Ca) is derived from either intermediate-felsic igneous rocks (sub-type Bi;  $X_{Mg} < 20\%$ ,  $X_{Ca} < 10\%$ ) or amphibolite-facies metasedimentary rocks (sub-type Bii). Type C garnet (high Mg, high Ca) is preferentially contained in high-grade metabasite (sub-type Ci) or ultramafic rocks such as pyroxenite and peridotite (sub-type Cii;  $X_{Mg} > 40\%$ ,  $X_{Ca} > 10\%$ ), and type D garnet (low Mg, very high Ca) in metasomatic rocks (skarn), very low-grade metabasite, and high-grade calc-silicate rocks.

The different origins of detrital garnet are also highlighted by the use of the Mn–Mg–Ca diagram, based on the observation that  $Mg^{2+}$  progressively substitutes for  $Mn^{2+}$  and  $Fe^{2+}$  in pyralspite garnet with increasing metamorphic temperature, whereas  $Ca^{2+}$  increases at increasing pressures [120,121].

### 3.7. Epidote Chemistry

For the classification of epidote-group minerals we used the Windows<sup>TM</sup> program WinEpclas developed by Yavuz and Yildirim [122] and based on the nomenclature recommended by the Commission on New Minerals and Mineral Names of the International Mineralogical Association. The structural formula of monoclinic epidote-group minerals can be expressed as  $A_1A_2M_1M_2M_3 [T_2O_7][TO_4](O_4)(O_{10})$ , where A1 = Ca,  $Mn^{2+}$ ; A2 = Ca, Sr, Pb,  $Ce^{3+}$ , (REE)<sup>3+</sup>; M1 = Mg,  $Fe^{2+}$ ,  $Mn^{2+}$ , Al,  $Fe^{3+}$ ,  $V^{3+}$ ,  $Mn^{3+}$ ,  $Cr^{3+}$ ; M2 = Al,  $Fe^{3+}$ ; M3 = Mg,  $Fe^{2+}$ ,  $Mn^{2+}$ , Al,  $Fe^{3+}$ ,  $V^{3+}$ ,  $Mn^{3+}$ ,  $Cr^{3+}$ ; T = Si; O4 =  $O^{2-}$ , F<sup>−</sup>; and O10 = OH<sup>−</sup>,  $O^{2-}$  [123]. The normalization scheme based on the  $\Sigma(A + M + T) = 8.0$  determines the mineral species on the basis of the dominant cations at sites A1, A2, M1, M2, and M3, and of anions at sites O4 and O10.

Zoisite, the orthorhombic polymorph of clinozoisite, cannot be distinguished chemically from its monoclinic polymorph clinozoisite, and is thus not considered as a distinct species by WinEpclas software.

### 3.8. Pyroxene Chemistry

The general formula of orthorhombic or monoclinic pyroxene can be expressed as  $ABZ_2O_6$ , where A = Ca,  $Fe^{2+}$ , Li, Mg,  $Mn^{2+}$ , Na, Zn; B = Al,  $Cr^{3+}$ ,  $Fe^{2+}$ ,  $Fe^{3+}$ , Mg,  $Mn^{2+}$ , Sc, Ti,  $V^{3+}$ ; Z = Al, Si. Composition of detrital pyroxene was calculated on the basis of six oxygen atoms in the chemical formula, using the software developed by Sturm [124]. The nomenclature follows the rules set in Morimoto et al. [125]. The prefixes “aluminian” or “sodian” are added for clinopyroxene with  $Al^{3+} > 0.1$  atoms per formula unit (a.p.f.u.) or  $Na^+ > 0.1$  a.p.f.u., respectively. The prefix “subsiliic” is added if  $Si^{4+}$  is  $< 1.75$  a.p.f.u. Most pyroxene grains belong to the Quad chemical group (i.e., plot in the classical pyroxene quadrilateral, part of the Ca–Mg–Fe classification triangle; [125]). The J parameter is twice Na a.p.f.u.; the Q parameter is Ca + Mg +  $Fe^{2+}$  a.p.f.u.

## 4. Heavy Mineral Sources

Transparent heavy-mineral suites in all analyzed samples mostly consist (84% on average) of amphibole (47%  $\pm$  17%), epidote (17%  $\pm$  9%), pyroxene (12%  $\pm$  9%), and garnet grains (9%  $\pm$  8%).

Heavy-mineral concentration results to be much higher in river sand derived from the Kohistan arc (19%–44%) than from the Ladakh arc (5%–20%), and higher in river sand derived from the Nanga Parbat massif (6%–17%) than from both Karakorum belt and Greater Himalaya (3%–9%). Heavy mineral concentration is remarkably high in dune sand of the Thal Desert (12%–26%; Table 1).

**Table 1.** Heavy-mineral assemblages in river sands of the Upper Indus catchment (end-member sources) and eolian dunes of the Thal Desert (sediment sink) performed by semi-automated Raman spectroscopy.

Sample	River/Dune	Domain	HMC	tHMC	Zrn	Tur	Rt	Ttn	Ap	Amp	Cpx	Opx	Ol	Zo
S1749	Hushe	Karakorum	4.8	2.5	2	0.2	1	9	6	60	5	0	0.5	0
S1748	Braldu	Karakorum	6.5	4.5	0.9	1	3	8	6	42	11	0	0.5	0.1
S1437	Hunza	Karakorum	2.9	1.5	0.5	2	9	10	5	45	8	0.2	0	0.2
S1438	Hispar	Karakorum	8.7	6.7	2	1	1	10	3	26	6	0	0.2	0
S4426	Stagmo	Ladakh arc	12.6	12.0	0.4	0.4	0.4	6	0.9	82	6	0	0	0
S4430	Domkar	Ladakh arc	9.7	8.1	2	0.3	1	7	1	73	6	0.3	0	0
S1439	Kandia	Kohistan arc	44.2	33.4	0	0	0.5	7	0.5	51	4	0	0.2	2
S1440	Swat	Kohistan arc	31.4	27.5	0.2	0	2	1	0.6	49	37	4	0	0
S4419	Zanskar	G. Himalaya	4.8	4.6	1	5	2	8	8	21	11	0	0.2	0
S1426	Nandihar	G. Himalaya	4.8	4.0	0.6	8	1	5	3	32	13	2	0	0.6
S1432	Astor	Nanga Parbat	17.9	16.9	0.2	1	2	1	0.3	64	6	0	0.2	0.6
S1462	Mankera	Thal Desert	21.2	15.3	0	1	1	4	0.3	40	10	1	0.5	0.5
S1463	Haidarabad	Thal Desert	24.2	18.6	0	0.4	2	6	1	36	11	3	0.4	0.9
S1470	Muzaffarghar	Thal Desert	26.4	17.7	0.3	0.8	2	4	1	35	13	2	1	0.7
S1474	Munda	Thal Desert	12.3	10.0	0.3	1	1	4	1	40	13	2	0.3	0.3
Sample	River/Dune	Domain	Czo	&Ep	Grt	Cld	St	And	Ky	Sil	&HM	Tot	%Amp	%Grt
S1749	Hushe	Karakorum	1	11	4	0	0	0	0	0.2	0.6	100.0	1.5	0.1
S1748	Braldu	Karakorum	5	11	7	1	0.4	0.8	0	0.4	1	100.0	1.9	0.3
S1437	Hunza	Karakorum	6	13	1	0	0.2	0.3	0	0	0.5	100.0	0.7	0.0
S1438	Hispar	Karakorum	9	15	26	0.2	0.5	0	0	0	0.2	100.0	1.7	1.7
S4426	Stagmo	Ladakh arc	0	3	0	0	0	0	0	0	0	100.0	9.9	0.0
S4430	Domkar	Ladakh arc	0.5	7	1	0	0	0	0	0	0.8	100.0	5.9	0.1
S1439	Kandia	Kohistan arc	22	10	2	0	0	0	0	0	0	100.0	17.1	0.7
S1440	Swat	Kohistan arc	2	4	0.6	0	0	0	0	0	0	100.0	13.5	0.2
S4419	Zanskar	G. Himalaya	0.3	11	21	0	0.3	0	0.5	9	1	100.0	1.0	1.0
S1426	Nandihar	G. Himalaya	1	2	22	0	2	0	8	0.6	0.4	100.0	1.3	0.9
S1432	Astor	Nanga Parbat	5	9	9	0	0.2	0.2	0.8	0.2	0.2	100.0	10.8	1.6
S1462	Mankera	Thal Desert	15	9	14	0.3	0.8	0	1	0.2	0.7	100.0	6.1	2.1
S1463	Haidarabad	Thal Desert	11	13	14	0	0.6	0.2	0.4	1	0	100.0	6.6	2.5
S1470	Muzaffarghar	Thal Desert	14	11	11	0	0.5	0	0.8	0.5	0.5	100.0	6.3	2.0
S1474	Munda	Thal Desert	11	12	10	0	0.6	0	1	0.3	0.1	100.0	4.0	1.0

On average, over 700 transparent heavy minerals were counted per sample (ranging from 275 for S4426 to 1300 for S1748; Supplementary Table S2). HMC = heavy mineral concentration; tHMC = transparent heavy mineral concentration; Zrn = zircon; Tur = tourmaline; Rt = rutile; Ttn = titanite; Ap = apatite; Amp = amphibole; Cpx = clinopyroxene; Opx = orthopyroxene; Ol = olivine; Zo = zoisite; Czo = clinozoisite; &Ep = allanite and other epidote-group minerals; Grt = garnet; Cld = chloritoid; St = staurolite; And = andalusite; Ky = kyanite; Sil = sillimanite; &HM = other transparent heavy minerals (monazite, anatase, brookite, prehnite, axinite, gahnite, barite, vesuvianite). Percentages of amphibole, garnet, epidote, and pyroxene on bulk samples are given in the four last columns to the right.

#### 4.1. Karakorum

The studied river sands derived from the Karakorum contain moderately poor to rich transparent-heavy-mineral suites dominated by amphibole, with subordinate epidote, clinopyroxene, titanite and rare clinozoisite, apatite, and garnet. The Hispar River, draining mid-crustal rocks rapidly exhumed in metamorphic domes of the Southern Karakorum Belt, carries the richest transparent-heavy-mineral suite containing subequal amounts of garnet and amphibole (Table 1).

Amphibole grains in sand of the upper Hushe River, which largely drains granitoid rocks, are mainly pargasite (52%), hastingsite (26%), and hornblende (Figure 3A). Garnet grains mainly plot in field Bi of the Fe + Mn–Mg–Ca plot and in the low P/T field of the Ca–Mg–Mn plot (Figure 4A), reflecting provenance from intermediate-felsic igneous rocks. Epidote-group minerals include abundant REE-rich allanite (11% on average) and detrital pyroxene is mainly diopside with subordinate augite with a low wollastonite (Wo) value and negligible orthopyroxene (Figures 5A and 6A).

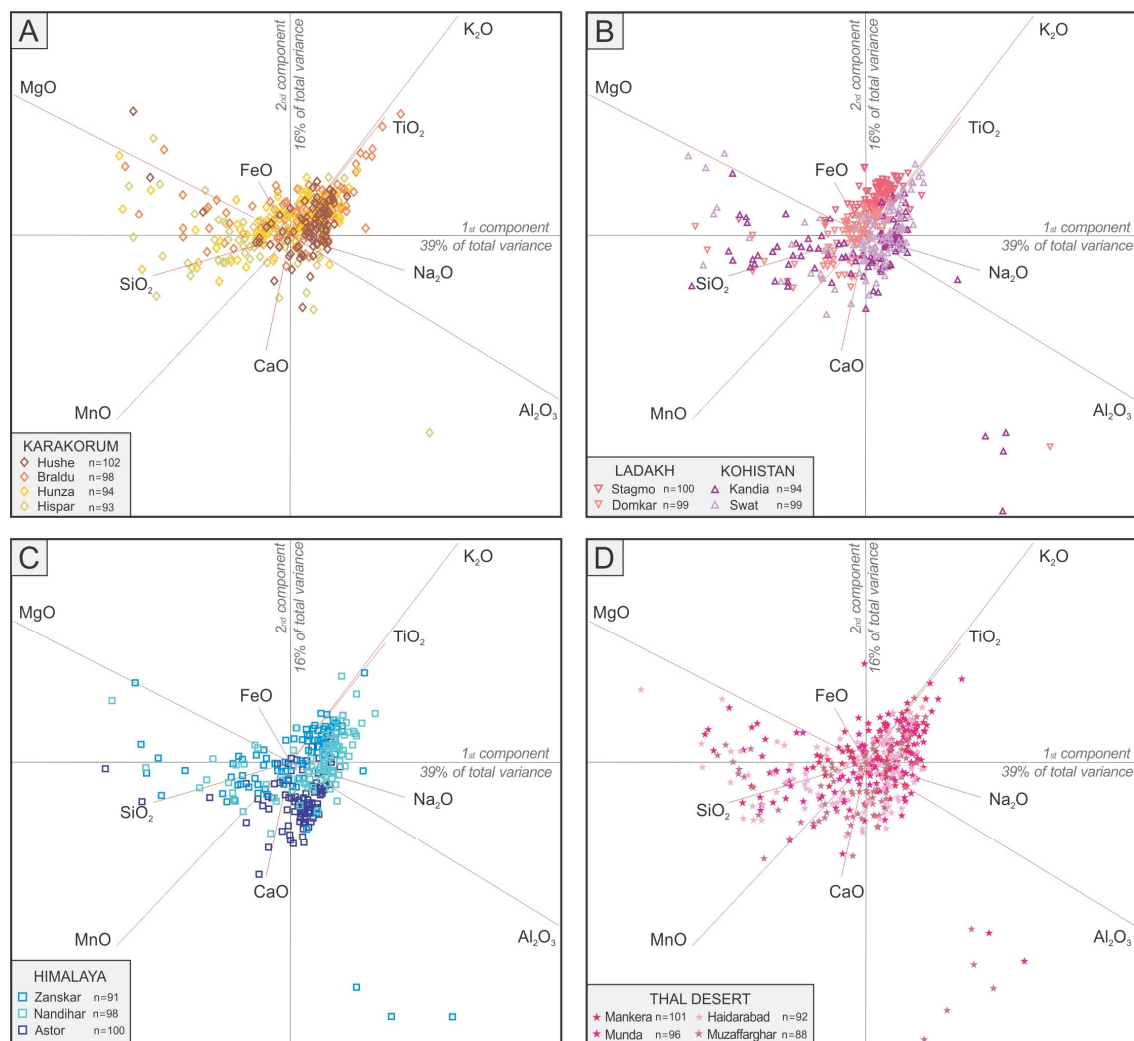


**Figure 3.** Chemical composition of detrital amphibole in river and eolian sands of northern Pakistan. All data were plotted in one single biplot [111], next separated into four panels to allow comparison between end-member sources (A = Karakprum, B = Ladakh and Kohistan arcs, C = Himalaya) and the sediment sink (D = Thal Desert).

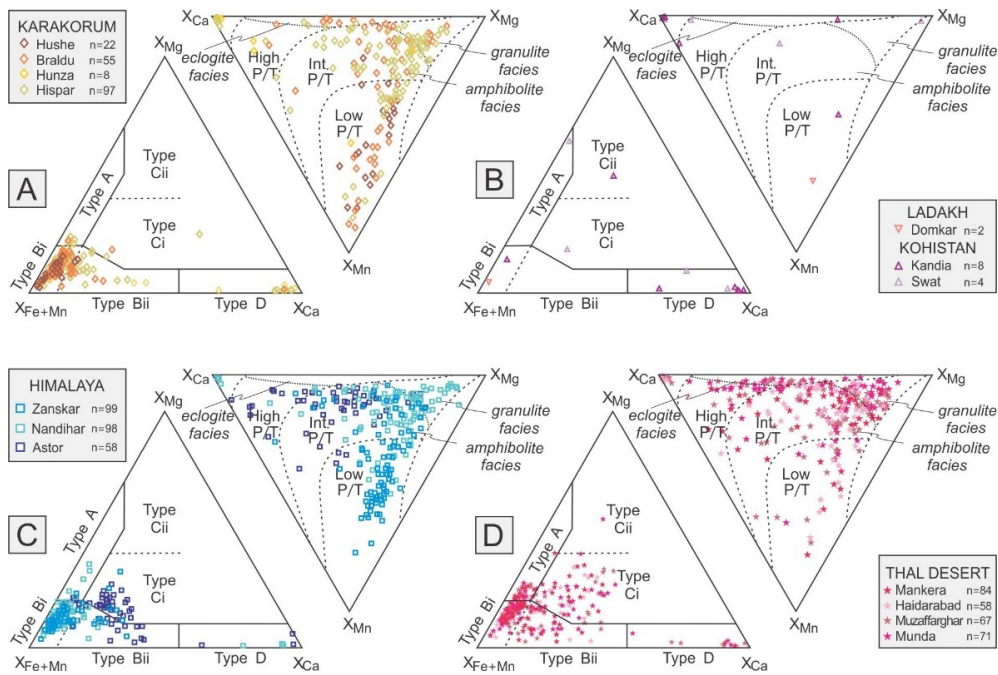


**Figure 4.** Chemical composition of detrital garnet in river sands of northern Pakistan (A = Karakorum, B = Ladakh and Kohistan arcs, C = Himalaya) and in the (D) Thal Desert. (Fe + Mn–Mg–Ca plot after Mange and Morton [5]; Ca–Mg–Mn plot after Win et al. [121]). XFe, XMg, XCa, XMn = molecular proportions of Fe<sup>2+</sup>, Mg, Ca, and Mn.

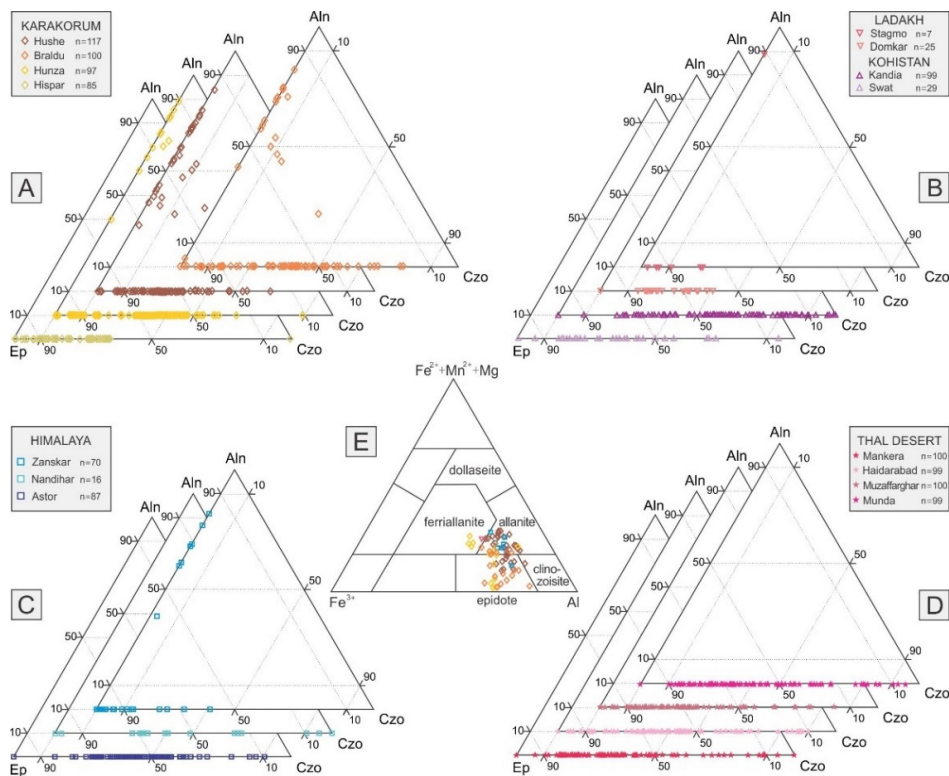


**Figure 5.** Chemical composition of detrital epidote-group minerals in river sands of northern Pakistan and in the Thal Desert. (A–D) The proportion of clinozoisite, allanite, and epidote were calculated as Al (atoms per formula unit (a.p.f.u.) – 2, if Al (a.p.f.u.) > 2 (otherwise the proportion was taken as zero), as rare earth elements (REE) (a.p.f.u.), and as 1–allanite–clinozoisite, respectively [126]. Aln: allanite; Ep: epidote; Czo: clinozoisite. (E) Classification of REE-bearing epidote grains after Kartashov [127].

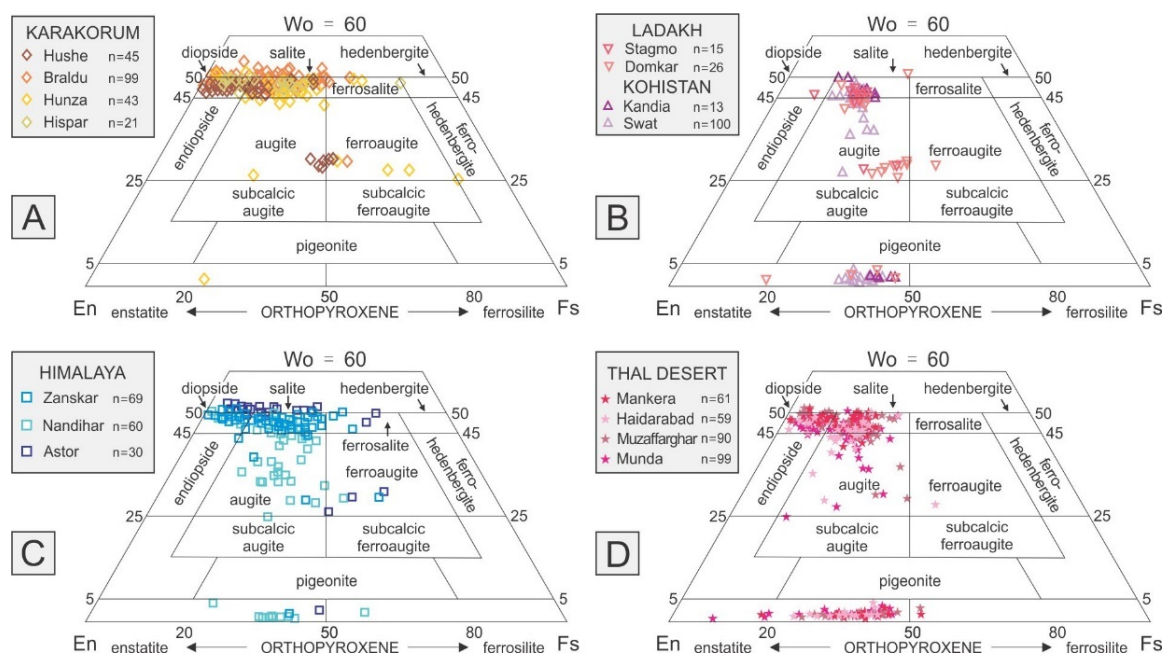


**Figure 6.** Chemical composition of detrital pyroxene in river sands of northern Pakistan (A = Karakorum, B = Ladakh and Kohistan arcs, C = Himalaya) and in the (D) Thal Desert. Pyroxene quadrilateral from Poldervaart and Hess [128] and Morimoto et al. [125]. Wo: Wollastonite ( $\text{Ca}_2\text{Si}_2\text{O}_6$ ); En: enstatite ( $\text{Mg}_2\text{Si}_2\text{O}_6$ ); Fs: ferrosilite ( $\text{Fe}_2\text{Si}_2\text{O}_6$ ).

Sand of the upper Braldu River draining the axial part of the Karakorum belt contains mainly hornblende prevailing over pargasite and actinolite, and mainly Bi with subordinate Bii garnet plotting in the low and intermediate P/T fields (Figure 4A). Epidote dominates over allanite and clinozoisite. Pyroxene is mostly diopside, largely derived from upper-amphibolite facies metasedimentary rocks (99%; Figure 6A). Similar mineralogical signatures characterize upper Hunza and Hispar sands, mainly derived from the Northern Karakorum sedimentary domain and from the Southern Karakorum belt, respectively. Hispar sand however lacks allanite (Figure 5A), whereas upper Hunza sand contains only a few garnet grains, dominantly of type D (Figure 4A), and some ferroaugite grains (Figure 6A).

#### 4.2. Ladakh and Kohistan Arcs

Stream sands derived from the Ladakh arc contain rich to very rich, amphibole-dominated transparent heavy-mineral suites including minor titanite, clinopyroxene, epidote, and only rare garnet (Figure 4B). Amphibole grains are mostly hornblende (~81% on average; Figure 3B), epidote is dominant (allanite is rare in Stagmo sand and absent in Domkar sand; Figure 5B), and detrital pyroxene is mainly diopside and augite (Figure 6B). Domkar sand includes a few orthopyroxene grains.

The very rich to extremely rich transparent heavy-mineral suites shed from the Kohistan arc are more varied (Table 1). Kandia sand yields mainly pargasite, hornblende, and actinolite among the amphibole group, abundant epidote-group minerals (mostly clinozoisite; Figure 5B), mostly high-Ca garnet of type D (Figure 4B), and only a few diopside and orthopyroxene grains (Figure 6B). In Swat sand, common detrital amphibole is mainly hornblende (42%), with minor pargasite and hastingsite, and rare actinolite and tschermakite. Clinopyroxene (diopside, minor augite) is abundant and orthopyroxene minor (Figure 6B). Epidote-group minerals are represented by epidote and clinozoisite (Figure 5B). The rare garnet grains are high in Ca and Mg (Figure 4B).

#### 4.3. Greater Himalaya

Rivers draining amphibolite-facies metamorphic rocks of the Greater Himalaya carry moderately rich transparent heavy-mineral suites including amphibole, garnet, clinopyroxene and epidote, with minor titanite, tourmaline, apatite, sillimanite, and kyanite (Table 1).

The Zaskar River, sourced from the topmost part of the Greater Himalaya and cutting across the Tethys Himalaya, carries pargasite and hornblende with minor hastingsite, mainly Bi garnet with a few Bii and Ci grains (Figure 4C), and dominant epidote with minor allanite (Figure 5C). Diopside accounts for the vast majority of pyroxene grains (Figure 6C).

Similar amphibole varieties characterize Nandihar river sand, which contains mainly Bi garnet with minor A, Bii, and D grains (Figure 4C), epidote-clinozoisite but no allanite (Figure 5C), and a higher proportion of augite (30%) and orthopyroxene (25%) (Figure 6C).

#### 4.4. Nanga Parbat

The very rich transparent-heavy-mineral suite of Astor River sand chiefly derived from the Nanga Parbat massif is dominated by amphibole with subordinate epidote-group minerals, garnet, and clinopyroxene (Table 1). Detrital amphibole is mainly hornblende with common tschermakite (14%) and minor pargasite (Figure 3C). Garnet grains are mainly Ci (57%) and minor Bii types (Figure 4C). Epidote and clinozoisite occur whereas allanite is lacking (Figure 5C), and detrital pyroxene is dominantly diopside with rare augite and orthopyroxene (Figure 6C).

### 5. Heavy-Mineral Provenance Tracers in Thal Desert Sand

Transparent-heavy-mineral suites of Thal Desert sand reflect the mineralogy of their diverse magmatic and metamorphic sources. As each source-rock domain contributes detrital species to the sediment load of the upper Indus River in different proportions, depending not only on exposure area and erosion rate but also on the different mineral concentrations (fertilities), every detrital mineral is expected to carry a distinct provenance signal (Figure 7). A source-rock domain may contribute one mineral (e.g., amphibole) in large proportion but another mineral (e.g., garnet) in negligible proportion; as a consequence, that domain will be over-represented in the detrital-amphibole spectrum but hardly seen in the detrital-garnet spectrum.

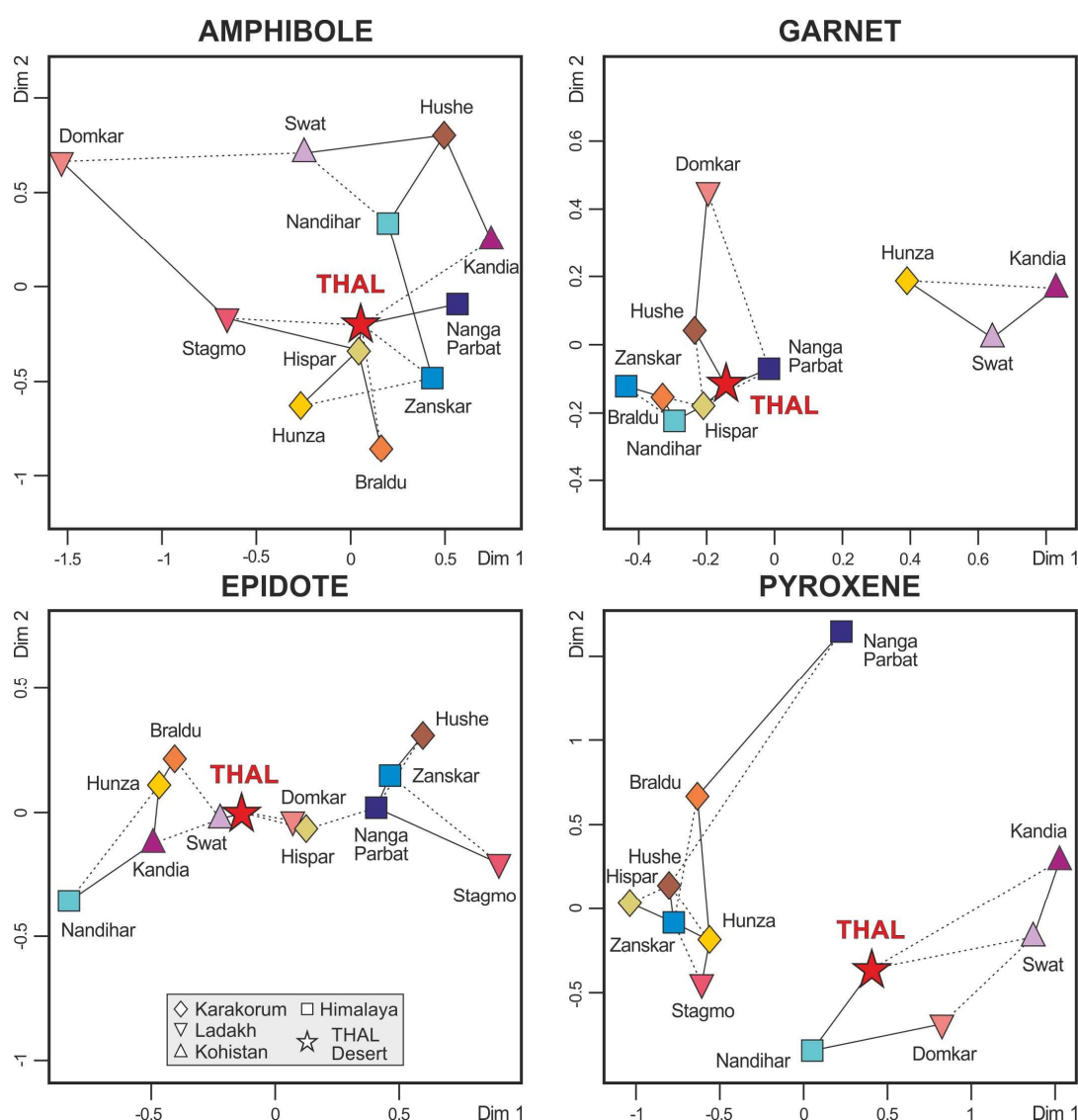


**Figure 7.** Multidimensional scaling maps based on the chemical signatures of the four studied mineral groups in river sands of northern Pakistan and in the Thal Desert (Supplementary Tables S7–S10). The four Thal dune samples are considered as subsamples of the same unitary population. Solid and dashed lines link closest and second-closest neighbors, respectively. The higher “stress” values (poorer fit) obtained for the amphibole (11.2%) and pyroxene maps (8.9%) than for the garnet (2.4%) and epidote maps (0.8%) largely reflect the higher number of varieties identified for amphibole (32) and pyroxene (39) than for epidote and garnet (six each). The four maps—plotted using the provenance package of Vermeesch et al. [129]—differ because different minerals are contained in markedly different proportions (fertilities) in different source-rock domains. Similarities among mineralogical spectra indicate the Kohistan arc as the main supplier of epidote and pyroxene, whereas amphibole and garnet were largely derived also from the Karakorum (Southern Karakorum gneiss domes drained by the Hispar River) and Himalaya (Nanga Parbat massif). The shape and color of sample symbols are same with those of Figures 3–6.

### 5.1. The Thal Desert as a Quaternary Sediment Sink

The very rich transparent-heavy-mineral suites of Thal Desert sand (tHMC  $15.4 \pm 3.9$ ) mainly consist of amphibole, with common epidote, clinozoisite, clinopyroxene, and garnet. Detrital amphibole includes mainly hornblende, subordinate pargasite, actinolite (11% on average), hastingsite, and minor

tschermakite (up to 5%; Figure 3D). Detrital garnet mainly consists of Bi grains with minor Ci (23%), Bii (18%), A (13%), and a few D grains (Figure 4D). Epidote-group minerals are mainly clinozoisite (54% on average) and epidote (Figure 5D). Detrital pyroxene is mainly diopside with common orthopyroxene (32% on average) and minor augite (Figure 6D).

The four studied dune samples are compositionally homogeneous (Table 1) and can thus be considered as subsamples of the same unitary population. Minor differences, however, are observed for instance between the adjacent Mankera and Haidarabad samples (Figure 1). Sample S1462 yielded more hornblende and more Bii than Ci garnets (20% vs. 18%), whereas sample S1463 yielded more hastingsite (27%), less Bii than Ci garnets (12% vs. 26%), and a lower diopside/augite ratio (Figures 8 and 9).

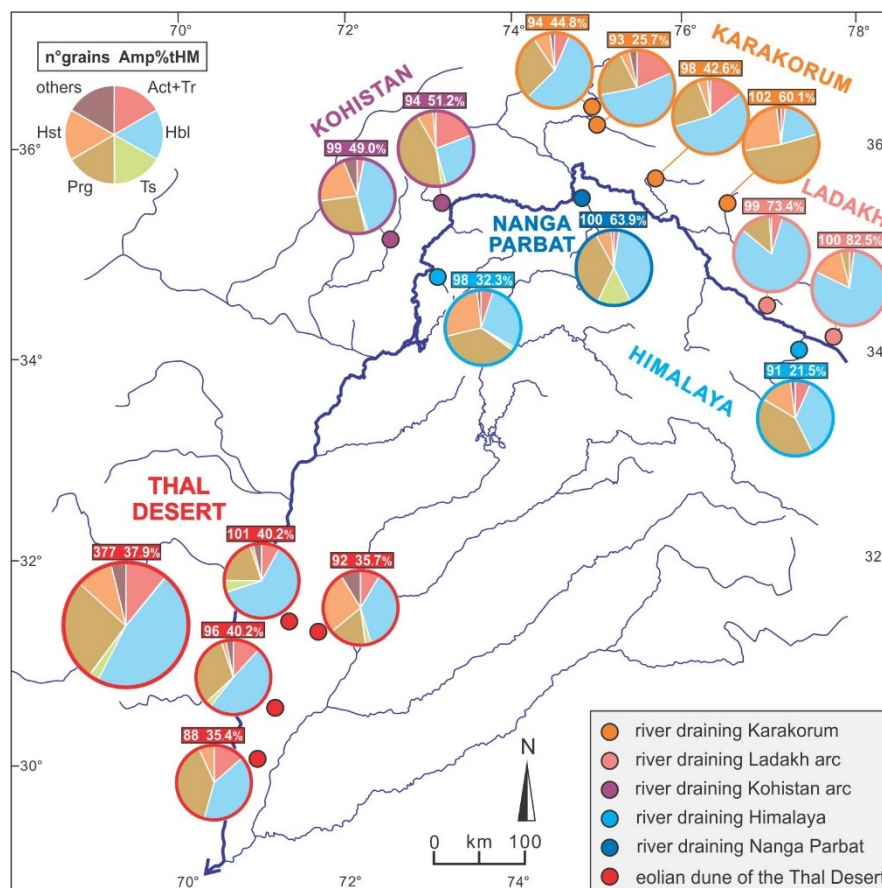


**Figure 8.** Calculated proportions of different varieties of detrital amphibole found in river and eolian sands of northern Pakistan. Act: actinolite; Hbl: hornblende; Hst: hastingsite; Prg: pargasite; Tr: tremolite; Ts: tschermakite.

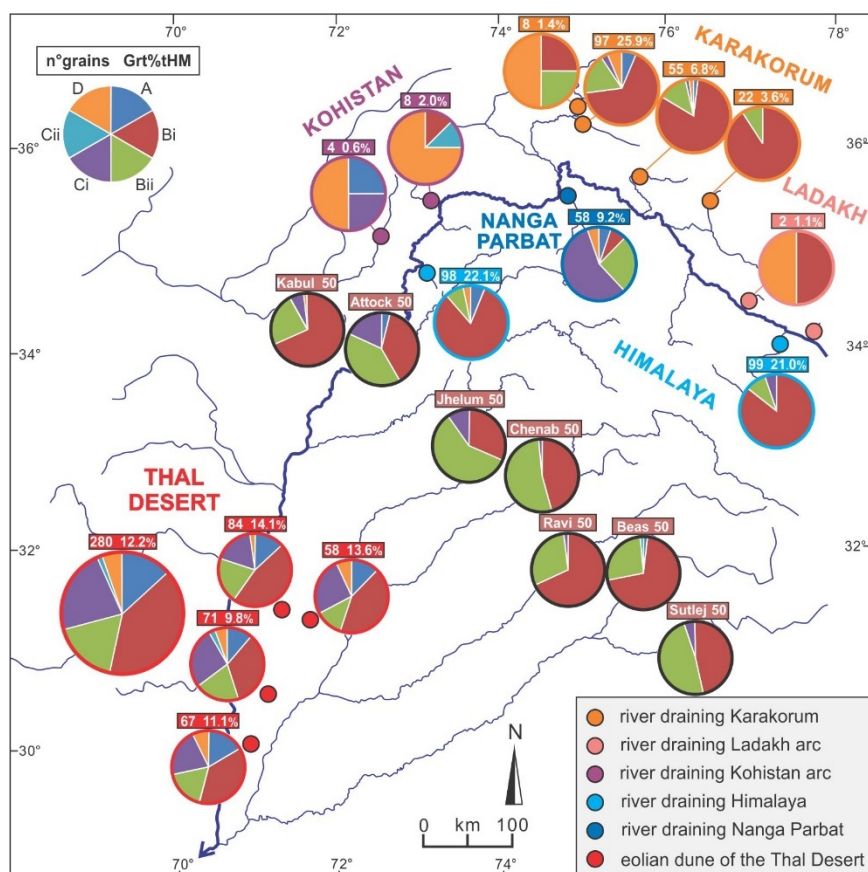


**Figure 9.** Calculated proportions of different varieties of detrital garnet (as defined in Mange and Morton, [5]) found in river and eolian sands of northern Pakistan. Data for Kabul, Indus, Jhelum, Chenab, Ravi, Beas, and Sutlej sands, circled in black, are from Alizai et al. [22]. Garnet types are explained in the text (Section 3.6).

## 5.2. Heavy Mineral Concentration and Provenance Estimates

A fundamental parameter in provenance analysis is represented by heavy-mineral concentration (HMC; [100,101]), which depends originally on the mineralogy and on the average density of parent rocks. The denser a rock is, the greater amount of dense minerals it contains and therefore can shed. Heavy-mineral concentration in sediments, however, can be modified even by an order of magnitude or more by hydraulic sorting during erosion, transport and sedimentation [106], or by chemical processes including weathering in soils and intrastratal dissolution during burial diagenesis [118,130]. Only in the absence of such environmental and diagenetic bias can terrigenous detritus be considered as produced purely by physical comminution and the mineralogy of daughter sand held to faithfully reflect the mineralogy of parent rocks. Under this strict assumption, the concentration (fertility) of each mineral can be determined for any specific source by the mineralogical analysis of daughter sand [15].

Our mineralogical dataset, integrated by data from Garzanti et al. [18] and Munack et al. [30], indicates that erosion in the diverse tectonic domains of the upper Indus catchment generate different amounts of heavy minerals. This depends principally on arc versus continental protoliths and crustal level exposed to erosion in each domain, because continental crust is more felsic and therefore less dense than arc crust, and because the Earth's crust is markedly stratified by density [131].

The very high transparent-heavy-mineral concentration in all of our four Thal dune-sand samples, which are not systematically enriched in densest minerals by selective-entrainment effects (Supplementary Table S1), points by itself to major heavy-mineral supply especially from dense mafic rocks exposed in deep tectonostratigraphic levels of the Kohistan arc and minor heavy-mineral supply from either the Karakorum or the Greater Himalaya. Similarity analysis [132] indicates that

heavy-mineral suites resembling more closely those of Thal Desert dunes are those of Braldu and Hispar sands derived from the Central-Southern Karakorum, whereas the least similar are those of stream sand derived from the Ladakh arc. Forward-mixing calculations based on heavy-mineral data shown in Table 1 (mathematical method explained in Weltje [133] and Garzanti et al., [134]) confirm the Kohistan arc and the Central-Southern Karakorum as major sources of sediment for the Thal dunes.

### 5.3. The Amphibole Signal

The composite amphibole population of Thal Desert sand includes hornblende as well as other species identified in sands carried by diverse mountain tributaries of the Indus River, pointing to mixing from several sources (Figure 8). The relatively high amount of actinolite suggests contribution from Karakorum and/or Kohistan, and the presence of tschermakite indicates significant supply from the Nanga Parbat.

The massive appearance of blue-green hornblende in Upper Miocene foreland-basin strata of northern Pakistan was used as an indicator of rapid exhumation of the Kohistan arc [135]. Geochemical data from Lee et al. [21] confirm the Kohistan arc as a major source of amphibole, whereas the Nanga Parbat massif together with the Himalayan belt and the Ladakh arc in the uppermost catchment were held to be minor contributors. Major supply from the Kohistan arc was principally ascribed to high fertility, whereas the Southern Karakorum Belt was identified as the dominant source of bulk sediment also based on Nd isotope fingerprints [24].

### 5.4. The Garnet Signal

As the studied rivers draining the Ladakh and Kohistan arcs carry little garnet, most of which are Ca-rich type-D grains, the arcs cannot be considered as significant sources for garnet (Figure 9). However, Thal Desert dunes contain common high-Mg Ci and A garnet grains, which may have been derived not only from Nanga Parbat and the Greater Himalaya, respectively, but also from granulite-facies metagabbros and metasedimentary rocks exposed in the southern part of the Kohistan arc drained by the Indus River. These high-grade rocks of the lower arc crust may in fact contain up to 20%–30% garnet [136,137]. High-Mn garnets plotting in the low P/T field are sporadic in Thal dunes, but common in all river sands derived from the Karakorum belt and the Greater Himalaya (Figure 4), which argues against dominant garnet contribution from these sources.

Geochemical data from Alizai et al. [22] indicate that garnet in Kabul sand has intermediate signatures between those of the Karakorum belt and the Kohistan arc, and that Punjab Rivers draining the Himalayan belt carry mainly Bi and Bii garnets with minor Ci grains (Figure 9). Type D garnet occurs in all geological domains drained by the Indus River upstream of the Thal Desert but not in Punjab tributaries (Figure 9), which do not contribute significant amounts of sediment to the Thal Desert. Mg-rich garnet derived from the Kohistan arc and subordinately from the Karakorum belt, characteristic of Indus sand, are still the mark of Thar Desert dunes in southern Pakistan, chiefly representing the wind-reworked alluvial fan of the Indus River [22].

### 5.5. The Epidote Signal

Although epidote has been generally used as a provenance tracer based on isotopic fingerprints [138,139], major element geochemistry also provides critical information. Most important, allanite grains were not detected in all four Thal sand samples, which precludes significant contribution from the Northern and Central Karakorum drained by the upper Hunza, upper Braldu, and upper Hushe rivers, and by the upper part of the Greater Himalaya drained by the Zanskar River (Figure 10). The abundance of clinozoisite favors instead major contribution from the Kohistan arc and possibly from the Southern Karakorum, drained by the Hispar which is the only Karakorum river that does not carry allanite. Subordinate supply from the Nanga Parbat massif, mainly shedding epidote, and from the Greater Himalaya in Pakistan, dominantly shedding clinozoisite, cannot be ruled out. Although zoisite cannot be identified from geochemical data by WinEpclas software [122], Raman spectroscopy revealed

its abundance in both Thal Desert and Kandia River sands (Table 1), confirming the Kohistan arc as a major source of detrital epidote for Thal dunes.

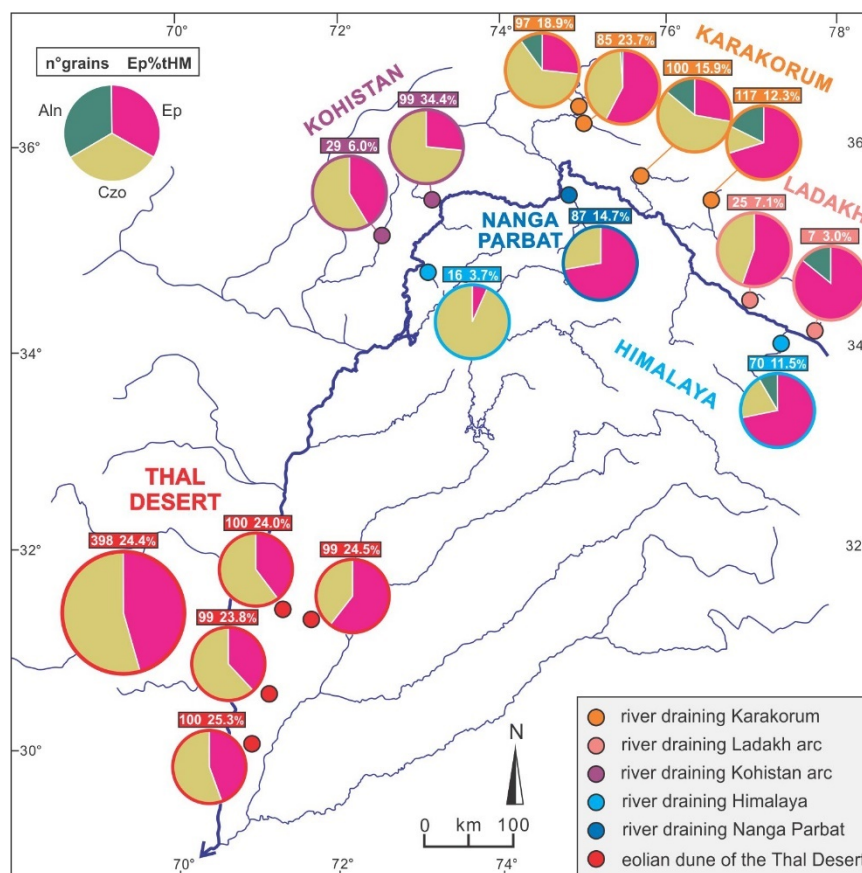


**Figure 10.** Calculated proportions of different varieties of detrital epidote-group minerals found in river and eolian sands of northern Pakistan. Note that Thal dunes, as well as sand from Kohistan and Nanga Parbat, lack allanite. Among Karakorum rivers, only the Hispar does not carry allanite, which singles out the Southern Karakorum as the only domain potentially representing a major source of epidote within the belt. Aln: allanite; Czo: clinozoisite; Ep: epidote.

### 5.6. The Pyroxene Signal

The abundance of orthopyroxene in Thal dunes points to dominant contribution from the Kohistan arc, with minor to negligible additional contributions from other sources (Figure 11). In fact, the Ladakh arc ( $W_o < 30$ ), the Karakorum belt (upper Hushe sand;  $W_o \sim 30$ ), and the Greater Himalaya (Nandihar sand;  $W_o < 40$ ) shed mostly Ca-poor augite (Figure 6), whereas augite grains in Thal Desert dunes are mostly Ca-rich ( $W_o > 40$ ). Detrital ferroaugite is negligible in Thal dunes, whereas it occurs in sand derived from Nanga Parbat, Greater Himalaya, and Karakorum belt (upper Hunza sand) (Figure 6).

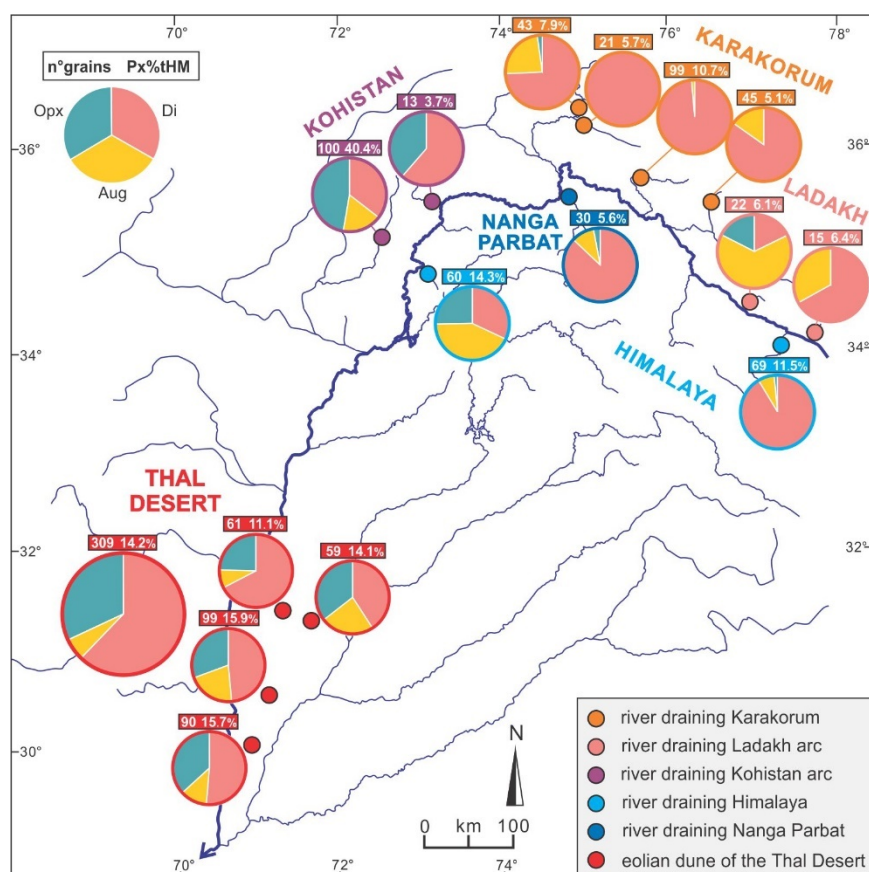


**Figure 11.** Calculated proportions of different varieties of detrital pyroxene found in river and eolian sands of northern Pakistan. Aug: augite ( $25 < Wo < 45$ ); Di: diopside ( $Wo > 45$ ); Opx: orthopyroxene ( $Wo < 5$ ); Wo: wollastonite.

## 6. Conclusions

Varietal studies of heavy minerals have long been proven to provide crucial information on sediment provenance. The present study focuses on the chemical composition of detrital amphibole, garnet, epidote, and pyroxene because these solid-solution series are the four dominant minerals in orogenic sediments worldwide. The rich minerochemical dataset produced is intended as a basis useful to discriminate among the diverse sources of detritus within the upper part of the Indus River catchment in northern Pakistan, upstream of its entry point in the Punjab foreland basin. Therefore, the thorough quantitative description of mineralogical signatures of Thal Desert dune sand, representing a relict sink of sediment entirely derived from the upper Indus River in the Quaternary, offers a complementary way to trace erosion patterns across the western Himalayan syntaxis and adjacent orogenic segments.

High-resolution analysis of Thal Desert dune sand indicates that the Kohistan arc has played the principal role as a source of heavy minerals, especially as pyroxene and epidote are concerned. The similarity among mineralogical spectra suggests that the Southern Karakorum gneiss domes undergoing fast exhumation and the Nanga Parbat massif were major suppliers of amphibole and garnet, reflecting high erosion rates in the western Himalaya syntaxis. Among other Himalayan domains, a minor amount of heavy minerals was supplied by the Greater Himalaya, whereas detritus from the Lesser Himalaya and Subhimalaya becomes significant in Indus sand only in southern Pakistan, downstream of the confluence with Punjab tributaries. The contrast between mineralogical fingerprints of Thal Desert sand, entirely derived from geological domains exposed around the western Himalayan syntaxis, and those of detritus carried by Punjab tributaries, which drain the Himalayan belt exclusively, can be exploited to assess how the relative contributions from these different parts of the Himalayan-Karakorum orogen to the Indus delta to huge deep-sea fan have changed through

time. Such a clear differentiation between Transhimalayan and Himalayan sources of detritus provides a semi-actualistic key that can be used, together with complementary compositional datasets and geological information, to make a step forward in the understanding of the erosional evolution of the Himalayan orogen and of landscape changes in the Punjab foreland basin as controlled by the complex interplay between climatic and tectonic forces in the recent and less recent past.

**Supplementary Materials:** The following are available online at <http://www.mdpi.com/2075-163X/9/8/457/s1>, Table S1: Sampling sites (including textural and geochemical information), Table S2: Heavy-mineral data obtained by semi-automated Raman spectroscopy, Table S3: Chemical composition of detrital amphiboles, Table S4: Chemical composition of detrital garnets, Table S5: Chemical composition of detrital epidote-group minerals, Table S6: Chemical composition of detrital pyroxenes, Table S7: Percentages of amphibole varieties in each sample, Table S8: Percentages of garnet varieties in each sample, Table S9: Percentages of epidote varieties in each sample, Table S10: Percentages of pyroxene varieties in each sample.

**Author Contributions:** Project design, E.G.; Data collection: W.L., P.G., S.A.; Semi-automated Raman counting and statistical analysis: A.R.; Writing and editing, W.L., E.G.

**Funding:** This study was supported financially by PRIN-MIUR (Progetto di Rilevante Interesse Nazionale, Ministero dell'Istruzione, dell'Università e della Ricerca) to E.Garzanti (2015EC9PJ5); MIUR – Dipartimenti di Eccellenza 2018–2022, Department of Earth and Environmental Sciences, University of Milano-Bicocca and State Scholarship Fund organized by China Scholarship Council (Grant No. 201606450012).

**Acknowledgments:** Heartfelt thanks to Giacomo Ghielmi and Filippo Lazzati, who collected Thal desert and Indus tributary sands in 2001, and to Mike Searle, Peter Clift, Jan Blöthe, and Henry Munack who provided additional samples from the upper Indus catchment. Careful constructive reviews by Carita Augustsson and other two reviewers are very gratefully acknowledged.

**Conflicts of Interest:** The authors declare no conflict of interest.

## References

1. Mange, M.A.; Wright, D.T. *Heavy Minerals in Use. Developments in Sedimentology Series*; Elsevier: Amsterdam, The Netherlands, 2007; Volume 58, 1283p.
2. Garzanti, E.; Vezzoli, G.; Lombardo, B.; Ando, S.; Mauri, E.; Monguzzi, S.; Russo, M. Collision-orogen provenance (western Alps): Detrital signatures and unroofing trends. *J. Geol.* **2004**, *112*, 145–164. [[CrossRef](#)]
3. Garzanti, E.; Resentini, A.; Vezzoli, G.; Ando, S.; Malusa, M.G.; Padoan, M.; Paparella, P. Detrital fingerprints of fossil continental-subduction zones (Axial Belt Provenance, European Alps). *J. Geol.* **2010**, *118*, 341–362. [[CrossRef](#)]
4. Garzanti, E.; Al-Juboury, A.I.; Zoleikhaei, Y.; Vermeesch, P.; Jotheri, J.; Akkoca, D.B.; Obaid, A.K.; Allen, M.B.; Ando, S.; Limonta, M. The Euphrates-Tigris-Karun river system: Provenance, recycling and dispersal of quartz-poor foreland-basin sediments in arid climate. *Earth Sci. Rev.* **2016**, *162*, 107–128. [[CrossRef](#)]
5. Mange, M.A.; Morton, A.C. Geochemistry of heavy minerals. In *Heavy Minerals in Use. Developments in Sedimentology Series*; Mange, M.A., Wright, D.T., Eds.; Elsevier: Amsterdam, The Netherlands, 2007; Volume 58, pp. 345–391. [[CrossRef](#)]
6. Krynine, P.D. The tourmaline group in sediments. *J. Geol.* **1946**, *54*, 65–87. [[CrossRef](#)]
7. Morton, A.C. A new approach to provenance studies: Electron microprobe analysis of detrital garnets from Middle Jurassic sandstones of the northern North Sea. *Sedimentology* **1985**, *32*, 553–566. [[CrossRef](#)]
8. Morton, A.C. Geochemical studies of heavy minerals and their application to provenance research. In *Developments in Sedimentary Provenance Studies*; Special Publication 57; Morton, A.C., Todd, S.P., Haughton, P.D.W., Eds.; Geological Society of London Publications: London, UK, 1991; pp. 31–45. [[CrossRef](#)]
9. von Eynatten, H.; Gaupp, R. Provenance of Cretaceous synorogenic sandstones in the Eastern Alps: Constraints from framework petrography, heavy mineral analysis and mineral chemistry. *Sediment. Geol.* **1999**, *124*, 81–111. [[CrossRef](#)]
10. Meinhold, G. Rutile and its applications in earth sciences. *Earth Sci. Rev.* **2010**, *102*, 1–28. [[CrossRef](#)]
11. Andò, S.; Morton, A.; Garzanti, E. Metamorphic grade of source rocks revealed by chemical fingerprints of detrital amphibole and garnet. In *Sediment Provenance Studies in Hydrocarbon Exploration and Production*; Special Publication 386; Scott, R.A., Smyth, H.R., Morton, A.C., Richardson, N., Eds.; Geological Society of London Publications: London, UK, 2014; pp. 351–371. [[CrossRef](#)]

12. Malusà, M.G.; Wang, J.; Garzanti, E.; Liu, Z.C.; Villa, I.M.; Wittmann, H. Trace-element and Nd-isotope systematics in detrital apatite of the Po river catchment: Implications for provenance discrimination and the lag-time approach to detrital thermochronology. *Lithos* **2017**, *290*, 48–59. [[CrossRef](#)]
13. von Eynatten, H.; Dunkl, I. Assessing the sediment factory: The role of single grain analysis. *Earth Sci. Rev.* **2012**, *115*, 97–120. [[CrossRef](#)]
14. Moecher, D.P.; Samson, S.D. Differential zircon fertility of source terranes and natural bias in the detrital zircon record: Implications for sedimentary provenance analysis. *Earth Planet. Sci. Lett.* **2006**, *247*, 252–266. [[CrossRef](#)]
15. Malusà, M.G.; Resentini, A.; Garzanti, E. Hydraulic sorting and mineral fertility bias in detrital geochronology. *Gondwana Res.* **2016**, *31*, 1–19. [[CrossRef](#)]
16. Garzanti, E.; Limonta, M.; Vezzoli, G.; An, W.; Wang, J.; Hu, X. Petrology and multimineral fingerprinting of modern sand generated from a dissected magmatic arc (Lhasa River, Tibet). In *Tectonics, Sedimentary Basins, and Provenance: A Celebration of William, R. Dickinson's Career*; Special Paper 540; Ingersoll, R.V., Lawton, T.F., Graham, S.A., Eds.; Geological Society of America: Boulder, CO, USA, 2018; pp. 197–221. [[CrossRef](#)]
17. Guo, R.; Hu, X.M.; Garzanti, E.; Lai, W.; Yan, B. Magmatic and metamorphic events in Himalaya and Tibet traced by geochronological and geochemical fingerprinting of detrital zircon, monazite, rutile, and titanite. *Earth Sci. Rev.* **2019**, in press.
18. Garzanti, E.; Vezzoli, G.; Ando, S.; Paparella, P.; Clift, P.D. Petrology of Indus River sands: A key to interpret erosion history of the Western Himalayan Syntaxis. *Earth Planet. Sci. Lett.* **2005**, *229*, 287–302. [[CrossRef](#)]
19. Clift, P.D.; Shimizu, N.; Layne, G.; Blusztajn, J.S.; Gaedicke, C.; Schluter, H.-U.; Clark, M.K.; Amjad, S. Development of the Indus Fan and its significance for the erosional history of the Western Himalaya and Karakoram. *Geol. Soc. Am. Bull.* **2001**, *113*, 1039–1051. [[CrossRef](#)]
20. Clift, P.D.; Giosan, L.; Carter, A.; Garzanti, E.; Galy, V.; Tabrez, A.R.; Pringle, M.; Campbell, I.H.; France-Lanord, C.; Blusztajn, J. Monsoon control over erosion patterns in the western Himalaya: Possible feed-back into the tectonic evolution. In *Monsoon Evolution and Tectonic-Climate Linkage in Asia*; Special Publications 342; Clift, P.D., Tada, R., Zheng, H., Eds.; Geological Society of London Publications: London, UK, 2010; pp. 185–218. [[CrossRef](#)]
21. Lee, J.I.; Clift, P.D.; Layne, G.; Blum, J.; Khan, A.A. Sediment flux in the modern Indus River inferred from the trace element composition of detrital amphibole grains. *Sediment. Geol.* **2003**, *160*, 243–257. [[CrossRef](#)]
22. Alizai, A.; Clift, P.D.; Still, J. Indus Basin sediment provenance constrained using garnet geochemistry. *J. Asian Earth Sci.* **2016**, *126*, 29–57. [[CrossRef](#)]
23. Garzanti, E.; Andò, S. Plate tectonics and heavy-mineral suites of modern sands. In *Heavy Minerals in Use. Developments in Sedimentology Series*; Mange, M.A., Wright, D.T., Eds.; Elsevier: Amsterdam, The Netherlands, 2007; Volume 58, pp. 741–763. [[CrossRef](#)]
24. Clift, P.D.; Lee, J.I.; Hildebrand, P.; Shimizu, N.; Layne, G.D.; Blusztajn, J.; Blum, J.D.; Garzanti, E.; Khan, A.A. Nd and Pb isotope variability in the Indus River System: Implications for sediment provenance and crustal heterogeneity in the Western Himalaya. *Earth Planet. Sci. Lett.* **2002**, *200*, 91–106. [[CrossRef](#)]
25. Alizai, A.; Clift, P.D.; Giosan, L.; Van Laningham, S.; Hinton, R.; Tabrez, A.R.; Danish, M.; The Edinburgh Ion Microprobe Facility (EIMF). Pb isotopic variability in the modern-Pleistocene Indus River system measured by ion microprobe in detrital K-feldspar grains. *Geochim. Cosmochim. Acta* **2001**, *75*, 4771–4795. [[CrossRef](#)]
26. Jonell, T.N.; Li, Y.; Blusztajn, J.; Giosan, L.; Clift, P.D. Signal or noise? Isolating grain size effects on Nd and Sr isotope variability in Indus delta sediment provenance. *Chem. Geol.* **2018**, *485*, 56–73. [[CrossRef](#)]
27. Clift, P.D.; Campbell, I.H.; Pringle, M.S.; Carter, A.; Zhang, X.; Hodges, K.V.; Khan, A.A.; Allen, C.M. Thermochronology of the modern Indus River bedload: New insight into the controls on the marine stratigraphic record. *Tectonics* **2004**, *23*, TC5013. [[CrossRef](#)]
28. Campbell, I.H.; Reiners, P.W.; Allen, C.M.; Nicolescu, S.; Upadhyay, R. He-Pb double dating of detrital zircons from the Ganges and Indus Rivers: Implication for quantifying sediment recycling and provenance studies. *Earth Planet. Sci. Lett.* **2005**, *237*, 402–432. [[CrossRef](#)]
29. Alizai, A.; Carter, A.; Clift, P.D.; Van Laningham, S.; Williams, J.C.; Kumar, R. Sediment provenance, reworking and transport processes in the Indus River by U–Pb dating of detrital zircon grains. *Glob. Planet. Chang.* **2011**, *76*, 33–55. [[CrossRef](#)]

30. Munack, H.; Korup, O.; Resentini, A.; Limonta, M.; Garzanti, E.; Blöthe, J.H.; Scherler, D.; Wittmann, H.; Kubik, P.W. Postglacial denudation of western Tibetan Plateau margin outpaced by long-term exhumation. *Geol. Soc. Am. Bull.* **2014**, *126*, 1580–1594. [[CrossRef](#)]
31. Alizai, A.; Hillier, S.; Clift, P.D.; Giosan, L.; Hurst, A.; Van Laningham, S.; Macklin, M. Clay mineral variations in Holocene terrestrial sediments from the Indus Basin. *Quat. Res.* **2012**, *77*, 368–381. [[CrossRef](#)]
32. Treloar, P.J.; Petterson, M.G.; Jan, M.Q.; Sullivan, M.A. A re-evaluation of the stratigraphy and evolution of the Kohistan arc sequence, Pakistan Himalaya: Implications for magmatic and tectonic arc-building processes. *J. Geol. Soc.* **1996**, *153*, 681–693. [[CrossRef](#)]
33. DiPietro, J.A.; Pogue, K.R. Tectonostratigraphic subdivisions of the Himalaya: A view from the west. *Tectonics* **2004**, *23*, TC5001. [[CrossRef](#)]
34. Pêcher, A.; Seeber, L.; Guillot, S.; Jouanne, F.; Kausar, A.; Latif, M.; Majid, A.; Mahéo, G.; Mugnier, J.L.; Rolland, Y.; et al. Stress field evolution in the northwest Himalayan syntaxis, northern Pakistan. *Tectonics* **2008**, *27*, TC6005. [[CrossRef](#)]
35. Burg, J.P. The Asia–Kohistan–India collision: Review and discussion. In *Arc-Continent Collision*; Brown, D., Ryan, P.D., Eds.; Springer: Berlin/Heidelberg, Germany, 2011; pp. 279–309. [[CrossRef](#)]
36. Khan, I.A.; Bridge, J.S.; Kappelman, J.; Wilson, R. Evolution of Miocene fluvial environments, eastern Potwar plateau, northern Pakistan. *Sedimentology* **1997**, *44*, 221–251. [[CrossRef](#)]
37. Hildebrand, P.R.; Noble, S.R.; Searle, M.P.; Waters, D.J.; Parrish, R.R. Old origin for an active mountain range: Geology and geochronology of the eastern Hindu Kush, Pakistan. *Geol. Soc. Am. Bull.* **2001**, *113*, 625–639. [[CrossRef](#)]
38. Ferguson, R.I. Sediment load of the Hunza River. In *The International Karakoram Project*; Miller, K.J., Ed.; Cambridge University Press: Cambridge, UK, 1984; Volume 2, pp. 581–598.
39. Ali, K.F.; de Boer, D.H. Factors controlling specific sediment yield in the upper Indus River basin, northern Pakistan. *Hydrol. Process.* **2008**, *22*, 3102–3114. [[CrossRef](#)]
40. Einsele, G.; Hinderer, M. Terrestrial sediment yield and the lifetimes of reservoirs, lakes, and larger basins. *Geol. Rundsch.* **1997**, *86*, 288–310. [[CrossRef](#)]
41. Tate, E.L.; Farquharson, F.K. Simulating reservoir management under the threat of sedimentation: The case of Tarbela Dam on the River Indus. *Water Resour. Manag.* **2000**, *14*, 191–208. [[CrossRef](#)]
42. Rehman, S.S.; Sabir, M.A.; Khan, J. Discharge characteristics and suspended load from rivers of Northern Indus Basin, Pakistan. *Geol. Bull. Univ. Peshawar* **1997**, *30*, 325–326.
43. Milliman, J.D.; Quraishee, G.S.; Beg, M.A.A. Sediment discharge from the Indus River to the ocean: Past, present, and future. In *Marine Geology and Oceanography of the Arabian Sea and Coastal Pakistan*; Haq, B.U., Milliman, J.D., Eds.; Van Nostrand Reynolds: New York, NY, USA, 1984; pp. 65–70.
44. Meadows, A.; Meadows, P.S. *The Indus River: Biodiversity, Resources, Humankind*; Oxford University Press: Oxford, UK, 1999.
45. Searle, M.P.; Khan, M.A.; Fraser, J.E.; Gough, S.J.; Jan, M.Q. The tectonic evolution of the Kohistan-Karakoram collision belt along the Karakoram Highway transect, north Pakistan. *Tectonics* **1999**, *18*, 929–949. [[CrossRef](#)]
46. Hildebrand, P.R.; Searle, M.P.; Khan, Z.; Van Heijst, H.J. Geological evolution of the Hindu Kush, NW Frontier Pakistan: Active margin to continent-continent collision zone. In *Tectonics of the Nanga Parbat Syntaxis and the Western Himalaya*; Special Publication 170; Khan, M.A., Treloar, P.J., Searle, M.P., Jan, M.Q., Eds.; Geological Society of London Publications: London, UK, 2000; pp. 277–293. [[CrossRef](#)]
47. Gaetani, M.; Garzanti, E.; Jadoul, F.; Nicora, A.; Tintori, A.; Pasini, M.; Khan, K.S.A. The north Karakoram side of the Central Asia geopuzzle. *Geol. Soc. Am. Bull.* **1990**, *102*, 54–62. [[CrossRef](#)]
48. Zanchi, A.; Gaetani, M. The geology of the Karakoram range, Pakistan: The new 1: 100 000 geological map of Central-Western Karakoram. *Ital. J. Geosci.* **2011**, *130*, 161–262. [[CrossRef](#)]
49. Crawford, M.B.; Searle, M.P. Field relationships and geochemistry of pre-collisional (India-Asia) granitoid magmatism in the central Karakoram, northern Pakistan. *Tectonophysics* **1992**, *206*, 171–192. [[CrossRef](#)]
50. Searle, M.P.; Parrish, R.R.; Thow, A.V.; Noble, S.R.; Phillips, R.J.; Waters, D.J. Anatomy, age and evolution of a collisional mountain belt: The Baltoro granite batholith and Karakoram Metamorphic Complex, Pakistani Karakoram. *J. Geol. Soc.* **2010**, *167*, 183–202. [[CrossRef](#)]
51. Searle, M.P.; Turril, R. Structural and thermal evolution of the Karakoram crust. *J. Geol. Soc.* **1991**, *148*, 65–82. [[CrossRef](#)]

52. Rolland, Y.; Mahéo, G.; Guillot, S.; Pêcher, A. Tectono-metamorphic evolution of the Karakorum metamorphic complex (Dassu-Askole area, NE Pakistan): Exhumation of mid-crustal HT–MP gneisses in a convergent context. *J. Metamorph. Geol.* **2001**, *19*, 717–737. [[CrossRef](#)]
53. Palin, R.M.; Searle, M.P.; Waters, D.J.; Horstwood, M.S.A.; Parrish, R.R. Combined thermobarometry and geochronology of peraluminous metapelites from the Karakoram metamorphic complex, North Pakistan; New insight into the tectonothermal evolution of the Baltoro and Hunza Valley regions. *J. Metamorph. Geol.* **2012**, *30*, 793–820. [[CrossRef](#)]
54. Treloar, P.J.; Rex, D.C.; Guise, P.G.; Coward, M.P.; Searle, M.P.; Windley, B.F.; Petterson, M.G.; Jan, M.Q.; Luff, I.W. K-Ar and Ar-Ar geochronology of the Himalayan collision in NW Pakistan: Constraints on the timing of suturing, deformation, metamorphism and uplift. *Tectonics* **1989**, *8*, 881–909. [[CrossRef](#)]
55. Gaetani, M.; Jadoul, F.; Erba, E.; Garzanti, E. Jurassic and Cretaceous orogenic events in the North Karakoram: Age constraints from sedimentary rocks. In *Himalayan Tectonics; Special Publications 74*; Treloar, P.J., Searle, M.P., Eds.; Geological Society of London Publications: London, UK, 1993; pp. 39–52. [[CrossRef](#)]
56. Robertson, A.H.; Collins, A.S. Shyok Suture Zone, N Pakistan: Late Mesozoic–Tertiary evolution of a critical suture separating the oceanic Ladakh Arc from the Asian continental margin. *J. Asian Earth Sci.* **2002**, *20*, 309–351. [[CrossRef](#)]
57. Rehman, H.U.; Seno, T.; Yamamoto, H.; Khan, T. Timing of collision of the Kohistan-Ladakh Arc with India and Asia: Debate. *Isl. Arc* **2011**, *20*, 308–328. [[CrossRef](#)]
58. Borneman, N.L.; Hodges, K.V.; Soest, M.C.; Bohon, W.; Wartho, J.A.; Cronk, S.S.; Ahmad, T. Age and structure of the Shyok suture in the Ladakh region of northwestern India: Implications for slip on the Karakoram fault system. *Tectonics* **2015**, *34*, 2011–2033. [[CrossRef](#)]
59. Garzanti, E.; Baud, A.; Mascle, G. Sedimentary record of the northward flight of India and its collision with Eurasia (Ladakh Himalaya, India). *Geodin. Acta* **1987**, *1*, 297–312. [[CrossRef](#)]
60. Najman, Y.; Jenks, D.; Godin, L.; Boudagher-Fadel, M.; Millar, I.; Garzanti, E.; Horstwood, M.; Bracciali, L. The Tethyan Himalayan detrital record shows that India-Asia terminal collision occurred by 54 Ma in the Western Himalaya. *Earth Planet. Sci. Lett.* **2017**, *459*, 301–310. [[CrossRef](#)]
61. Jan, M.Q.; Howie, R.A. The mineralogy and geochemistry of the metamorphosed basic and ultrabasic rocks of the Jijal complex, Kohistan, NW Pakistan. *J. Petrol.* **1981**, *22*, 85–126. [[CrossRef](#)]
62. Jagoutz, O.; Müntener, O.; Ulmer, P.; Pettke, T.; Burg, J.P.; Dawood, H.; Hussain, S. Petrology and mineral chemistry of lower crustal intrusions: The Chilas Complex, Kohistan (NW Pakistan). *J. Petrol.* **2007**, *48*, 1895–1953. [[CrossRef](#)]
63. Dhuime, B.; Bosch, D.; Garrido, C.J.; Bodinier, J.L.; Bruguiet, O.; Hussain, S.S.; Dawood, H. Geochemical architecture of the lower-to middle-crustal section of a paleo-island arc (Kohistan Complex, Jijal–Kamila area, northern Pakistan): Implications for the evolution of an oceanic subduction zone. *J. Petrol.* **2009**, *50*, 531–569. [[CrossRef](#)]
64. Honegger, K.; Dietrich, V.; Frank, W.; Gansser, A.; Thöni, M.; Trommsdorff, V. Magmatism and metamorphism in the Ladakh Himalayas (the Indus-Tsangpo suture zone). *Earth Planet. Sci. Lett.* **1982**, *60*, 253–292. [[CrossRef](#)]
65. Weinberg, R.F.; Dunlap, W.J. Growth and deformation of the Ladakh Batholith, Northwest Himalayas: Implications for timing of continental collision and origin of calc-alkaline batholiths. *J. Geol.* **2000**, *108*, 303–320. [[CrossRef](#)] [[PubMed](#)]
66. Garzanti, E.; Van Haver, T. The Indus clastics: Forearc basin sedimentation in the Ladakh Himalaya (India). *Sediment. Geol.* **1988**, *59*, 237–249. [[CrossRef](#)]
67. Henderson, A.L.; Najman, Y.; Parrish, R.; Boudagher-Fadel, M.; Barford, D.; Garzanti, E.; Andò, S. Geology of the Cenozoic Indus Basin sedimentary rocks: Paleoenvironmental interpretation of sedimentation from the western Himalaya during the early phases of India-Eurasia collision. *Tectonics* **2010**, *29*, TC6015. [[CrossRef](#)]
68. Anczkiewicz, R.; Burg, J.-P.; Hussain, S.S.; Dawood, H.; Ghazanfar, M.; Chaudhry, M. Stratigraphy and structure of the Indus Suture in the lower Swat, Pakistan, NW Himalaya. *J. Asian Earth Sci.* **1998**, *16*, 225–238. [[CrossRef](#)]
69. Mahéo, G.; Fayoux, X.; Guillot, S.; Garzanti, E.; Capiez, P.; Mascle, G. Relicts of an intra-oceanic arc in the Sapi-Shergol mélange zone (Ladakh, NW Himalaya, India): Implications for the closure of the Neo-Tethys Ocean. *J. Asian Earth Sci.* **2006**, *26*, 695–707. [[CrossRef](#)]
70. DeCelles, P.; Kapp, P.; Gehrels, G.; Ding, L. Paleocene-Eocene foreland basin evolution in the Himalaya of southern Tibet and Nepal: Implications for the age of initial India-Asia collision. *Tectonics* **2014**, *33*, 824–849. [[CrossRef](#)]

71. Hu, X.; Garzanti, E.; Wang, J.; Huang, W.; An, W.; Webb, A. The timing of India-Asia collision onset—Facts, theories, controversies. *Earth Sci. Rev.* **2016**, *160*, 264–299. [[CrossRef](#)]
72. Ratschbacher, L.; Frisch, W.; Liu, G.; Chen, C. Distributed deformation in southern and western Tibet during and after the India-Asia collision. *J. Geophys. Res. Solid Earth* **1994**, *99*, 19917–19945. [[CrossRef](#)]
73. Searle, M.; Corfield, R.I.; Stephenson, B.E.N.; McCarron, J.O.E. Structure of the North Indian continental margin in the Ladakh–Zaskar Himalayas: Implications for the timing of obduction of the Spontang ophiolite, India-Asia collision and deformation events in the Himalaya. *Geol. Mag.* **1997**, *134*, 297–316. [[CrossRef](#)]
74. Gaetani, M.; Garzanti, E. Multicyclic history of the Northern India continental margin (Northwestern Himalaya)(1). *AAPG Bull.* **1991**, *75*, 1427–1446.
75. Sciunnach, D.; Garzanti, E. Subsidence history of the Tethys Himalaya. *Earth Sci. Rev.* **2012**, *111*, 179–198. [[CrossRef](#)]
76. Pognante, U.T.; Lombardo, B. Metamorphic evolution of the High Himalayan crystallines in SE Zaskar, India. *J. Metamorph. Geol.* **1989**, *7*, 9–17. [[CrossRef](#)]
77. Herren, E. Zaskar shear zone: Northeast-southwest extension within the Higher Himalayas (Ladakh, India). *Geology* **1987**, *15*, 409–413. [[CrossRef](#)]
78. Steck, A. Geology of the NW Indian Himalaya. *Eclogae Geol. Helv.* **2003**, *96*, 147–196. [[CrossRef](#)]
79. Greco, A.; Spencer, D.A. A section through the Indian plate, Kaghan valley, NW Himalaya, Pakistan. In *Himalayan Tectonics*; Special Publications 74; Treloar, P.J., Searle, M.P., Eds.; Geological Society of London Publications: London, UK, 1993; pp. 221–236. [[CrossRef](#)]
80. Vannay, J.C.; Grasemann, B.; Rahn, M.; Frank, W.; Carter, A.; Baudraz, V.; Cosca, M. Miocene to Holocene exhumation of metamorphic crustal wedges in the NW Himalaya: Evidence for tectonic extrusion coupled to fluvial erosion. *Tectonics* **2004**, *23*, TC1014. [[CrossRef](#)]
81. Bossart, P.; Ottiger, R. Rocks of the Murree Formation in northern Pakistan: Indicators of a descending foreland basin of late Paleocene to middle Eocene age. *Eclogae Geol. Helv.* **1989**, *82*, 133–165.
82. Najman, Y.; Garzanti, E. Reconstructing early Himalayan tectonic evolution and paleogeography from Tertiary foreland basin sedimentary rocks, northern India. *Geol. Soc. Am. Bull.* **2000**, *112*, 435–449. [[CrossRef](#)]
83. White, N.; Pringle, M.; Garzanti, E.; Bickle, M.; Najman, Y.; Chapman, H.; Friend, P. Constraints on the exhumation and erosion of the High Himalayan slab, NW India, from foreland basin deposits. *Earth Planet. Sci. Lett.* **2002**, *195*, 29–44. [[CrossRef](#)]
84. Zeitler, P.K.; Chamberlain, C.P.; Smith, H.A. Synchronous anatexis, metamorphism, and rapid denudation at Nanga Parbat (Pakistan Himalaya). *Geology* **1993**, *21*, 347–350. [[CrossRef](#)]
85. Chamberlain, C.P.; Zeitler, P.K.; Barnett, D.E.; Winslow, D.; Poulson, S.R.; Leahy, T.; Hammer, J.E. Active hydrothermal systems during the recent uplift of Nanga Parbat, Pakistan Himalaya. *J. Geophys. Res. Solid Earth* **1995**, *100*, 439–453. [[CrossRef](#)]
86. Zeitler, P.K.; Chamberlain, C.P. Petrogenetic and tectonic significance of young leucogranites from the northwestern Himalaya, Pakistan. *Tectonics* **1991**, *10*, 729–741. [[CrossRef](#)]
87. Schneider, D.A.; Zeitler, P.K.; Kidd, W.S.F.; Edwards, M.A. Geochronologic constraints on the tectonic evolution and exhumation of Nanga Parbat, western Himalaya syntaxis, revisited. *J. Geol.* **2001**, *109*, 563–583. [[CrossRef](#)]
88. Burbank, D.W.; Leland, J.; Fielding, E.; Anderson, R.S.; Brozovic, N.; Reid, M.R.; Duncan, C. Bedrock incision, rock uplift and threshold hillslopes in the northwestern Himalayas. *Nature* **1996**, *379*, 505–510. [[CrossRef](#)]
89. Shroder, J.F.; Bishop, M.P. Unroofing of Nanga Parbat Himalaya. In *Tectonics of the Nanga Parbat Syntaxis and the Western Himalaya*; Special Publication 170; Khan, M.A., Treloar, P.J., Searle, M.P., Jan, M.Q., Eds.; Geological Society of London Publications: London, UK, 2000; pp. 163–179. [[CrossRef](#)]
90. Whittington, A.G. Exhumation overrated at Nanga Parbat, northern Pakistan. *Tectonophysics* **1996**, *260*, 215–226. [[CrossRef](#)]
91. Moore, M.A.; England, P.C. On the inference of denudation rates from cooling ages of minerals. *Earth Planet. Sci. Lett.* **2001**, *185*, 265–284. [[CrossRef](#)]
92. Zeitler, P.K.; Meltzer, A.S.; Koons, P.O.; Craw, D.; Hallet, B.; Chamberlain, C.P.; Kidd, W.S.; Park, S.K.; Seeber, L.; Bishop, M.; et al. Erosion, Himalayan geodynamics, and the geomorphology of metamorphism. *GSA Today* **2001**, *11*, 4–9. [[CrossRef](#)]

93. Johnson, N.M.; Stix, J.; Tauxe, L.; Cervený, P.F.; Tahirkheli, R.A. Paleomagnetic chronology, fluvial processes, and tectonic implications of the Siwalik deposits near Chinji village, Pakistan. *J. Geol.* **1985**, *93*, 27–40. [[CrossRef](#)]
94. Najman, Y.; Garzanti, E.; Pringle, M.; Bickle, M.; Stix, J.; Khan, I. Early-Middle Miocene paleodrainage and tectonics in the Pakistan Himalaya. *Geol. Soc. Am. Bull.* **2003**, *115*, 1265–1277. [[CrossRef](#)]
95. Burbank, D.W.; Beck, R.A.; Mulder, T. The Himalayan foreland basin. In *The Tectonic Evolution of Asia (World and Regional Geology)*; Yin, A., Harrison, T.M., Eds.; Cambridge University Press: Cambridge, UK, 1996; pp. 149–188.
96. Nickson, R.T.; McArthur, J.M.; Shrestha, B.; Kyaw-Myint, T.O.; Lowry, D. Arsenic and other drinking water quality issues, Muzaffargarh District, Pakistan. *Appl. Geochem.* **2005**, *20*, 55–68. [[CrossRef](#)]
97. Ingersoll, R.V. Actualistic sandstone petrofacies: Discriminating modern and ancient source rocks. *Geology* **1990**, *18*, 733–736. [[CrossRef](#)]
98. Garzanti, E. The Himalayan foreland basin from collision onset to the present: A sedimentary-petrology perspective. In *Himalayan Tectonics: A Modern Synthesis*; Special Publication 483; Treloar, P., Searle, M.P., Eds.; Geological Society of London Publications: London, UK, 2019. [[CrossRef](#)]
99. Andò, S.; Garzanti, E. Raman spectroscopy in heavy-mineral studies. In *Sediment Provenance Studies in Hydrocarbon Exploration and Production*; Special Publication 386; Scott, R.A., Smyth, H.R., Morton, A.C., Richardson, N., Eds.; Geological Society of London Publications: London, UK, 2013; pp. 395–412. [[CrossRef](#)]
100. Garzanti, E.; Andò, S. Heavy-mineral concentration in modern sands: Implications for provenance interpretation. In *Heavy Minerals in Use; Developments in Sedimentology*; Mange, M.A., Wright, D.T., Eds.; Elsevier: Amsterdam, The Netherlands, 2007; Volume 58, pp. 517–545. [[CrossRef](#)]
101. Garzanti, E.; Andò, S. Heavy Minerals for Junior Woodchucks. *Minerals* **2019**, *9*, 148. [[CrossRef](#)]
102. Rubey, W.W. The size-distribution of heavy minerals within a water-laid sandstone. *J. Sediment. Petrol.* **1933**, *3*, 3–29. [[CrossRef](#)]
103. Garzanti, E.; Andò, S.; Vezzoli, G. Settling-equivalence of detrital minerals and grain-size dependence of sediment composition. *Earth Planet. Sci. Lett.* **2008**, *273*, 138–151. [[CrossRef](#)]
104. Briggs, L.I.; McCulloch, D.S.; Moser, F. The hydraulic shape of sand particles. *J. Sediment. Petrol.* **1962**, *32*, 645–656. [[CrossRef](#)]
105. Komar, P.D. The entrainment, transport and sorting of heavy minerals by waves and currents. In *Heavy Minerals in Use; Developments in Sedimentology Series*; Mange, M.A., Wright, D.T., Eds.; Elsevier: Amsterdam, The Netherlands, 2007; Volume 58, pp. 3–48. [[CrossRef](#)]
106. Garzanti, E.; Andò, S.; Vezzoli, G. Grain-size dependence of sediment composition and environmental bias in provenance studies. *Earth Planet. Sci. Lett.* **2009**, *277*, 422–432. [[CrossRef](#)]
107. Taylor, S.R.; McLennan, S.M. The geochemical evolution of the continental crust. *Rev. Geophys.* **1995**, *33*, 241–265. [[CrossRef](#)]
108. Rudnick, R.L.; Gao, S. Composition of the continental crust. In *Treatise on Geochemistry, The Crust*; Rudnick, R.L., Holland, H.D., Turekian, K.K., Eds.; Elsevier Pergamon: Oxford, UK, 2003; Volume 3, pp. 1–64. [[CrossRef](#)]
109. Vermeesch, P. How many grains are needed for a provenance study? *Earth Planet. Sci. Lett.* **2004**, *224*, 441–451. [[CrossRef](#)]
110. Vermeesch, P.; Garzanti, E. Making geological sense of ‘Big Data’ in sedimentary provenance analysis. *Chem. Geol.* **2015**, *409*, 20–27. [[CrossRef](#)]
111. Gabriel, K.R. The biplot graphic display of matrices with application to principal component analysis. *Biometrika* **1971**, *58*, 453–467. [[CrossRef](#)]
112. Hawthorne, F.C.; Oberti, R.; Harlow, G.E.; Maresch, W.V.; Martin, R.F.; Schumacher, J.C.; Welch, M.D. Nomenclature of the amphibole supergroup. *Am. Mineral.* **2012**, *97*, 2031–2048. [[CrossRef](#)]
113. Oberti, R.; Cannillo, E.; Toscani, G. How to name amphiboles after the IMA2012 report: Rules of thumb and a new PC program for monoclinic amphiboles. *Period. Mineral.* **2012**, *81*, 257–267. [[CrossRef](#)]
114. Locock, A.J. An Excel spreadsheet to classify chemical analyses of amphiboles following the IMA 2012 recommendations. *Comput. Geosci.* **2014**, *62*, 1–11. [[CrossRef](#)]
115. Locock, A.J. An Excel spreadsheet to recast analyses of garnet into end-member components, and a synopsis of the crystal chemistry of natural silicate garnets. *Comput. Geosci.* **2008**, *34*, 1769–1780. [[CrossRef](#)]

116. Morton, A.C.; Hallsworth, C. Stability of detrital heavy minerals during burial diagenesis. In *Heavy Minerals in Use; Developments in Sedimentology Series*; Mange, M.A., Wright, D.T., Eds.; Elsevier: Amsterdam, The Netherlands, 2007; Volume 58, pp. 215–245. [[CrossRef](#)]
117. Andò, S.; Garzanti, E.; Padoan, M.; Limonta, M. Corrosion of heavy minerals during weathering and diagenesis: A catalog for optical analysis. *Sediment. Geol.* **2012**, *280*, 165–178. [[CrossRef](#)]
118. Garzanti, E.; Ando, S.; Limonta, M.; Fielding, L.; Najman, Y. Diagenetic control on mineralogical suites in sand, silt, and mud (Cenozoic Nile Delta): Implications for provenance reconstructions. *Earth Sci. Rev.* **2018**, *185*, 122–139. [[CrossRef](#)]
119. Morton, A.; Hallsworth, C.; Chalton, B. Garnet compositions in Scottish and Norwegian basement terrains: A framework for interpretation of North Sea sandstone provenance. *Mar. Petrol. Geol.* **2004**, *21*, 393–410. [[CrossRef](#)]
120. Teraoka, Y.; Suzuki, M.; Kawakami, K. Provenance of Cretaceous and Paleogene sediments in the median zone of Southwest Japan. *Bull. Geol. Surv. Jpn.* **1998**, *49*, 395–411. [[CrossRef](#)]
121. Win, K.S.; Takeuchi, M.; Tokiwa, T. Changes in detrital garnet assemblages related to transpressive uplifting associated with strike-slip faulting: An example from the Cretaceous System in Kii Peninsula, Southwest Japan. *Sediment. Geol.* **2007**, *201*, 412–431. [[CrossRef](#)]
122. Yavuz, F.; Yildirim, D.K. A Windows program for calculation and classification of epidote-supergroup minerals. *Period. Mineral.* **2018**, *87*, 269–285. [[CrossRef](#)]
123. Armbruster, T.; Bonazzi, P.; Akasaka, M.; Bermanec, V.; Chopin, C.; Gieré, R.; Heuss-Assbichler, S.; Liebscher, A.; Menchetti, S.; Pan, Y.; et al. Recommended nomenclature of epidote-group minerals. *Eur. J. Mineral.* **2006**, *18*, 551–567. [[CrossRef](#)]
124. Sturm, R. PX-NOM—An interactive spreadsheet program for the computation of pyroxene analyses derived from the electron microprobe. *Comput. Geosci.* **2002**, *28*, 473–483. [[CrossRef](#)]
125. Morimoto, N.; Fabries, J.; Ferguson, A.K.; Ginzburg, I.V.; Ross, M.; Seifert, F.A.; Zussman, J.; Aoki, K.; Gottardi, G. Nomenclature of pyroxenes. *Miner. Petrol.* **1988**, *39*, 55–76. [[CrossRef](#)]
126. Graser, G.; Markl, G. Ca-rich ilvaite–epidote–hydrogarnet endoskarns: A record of late-magmatic fluid influx into the Persodic Ilímaussaq Complex, South Greenland. *J. Petrol.* **2007**, *49*, 239–265. [[CrossRef](#)]
127. Kartashov, P.M. Classification diagram for REE-bearing members of the epidote group based on crystallochemical data. In Proceedings of the Workshop on Accessory Minerals, Warsaw, Poland, 25–26 September 2014; pp. 19–21.
128. Poldervaart, A.; Hess, H.H. Pyroxenes in the crystallization of basaltic magma. *J. Geol.* **1951**, *59*, 472–489. [[CrossRef](#)]
129. Vermeesch, P.; Resentini, A.; Garzanti, E. An R package for statistical provenance analysis. *Sediment. Geol.* **2016**, *336*, 14–25. [[CrossRef](#)]
130. Garzanti, E.; Padoan, M.; Andò, S.; Resentini, A.; Vezzoli, G.; Lustrino, M. Weathering and relative durability of detrital minerals in equatorial climate: Sand petrology and geochemistry in the East African Rift. *J. Geol.* **2013**, *121*, 547–580. [[CrossRef](#)]
131. Garzanti, E.; Andò, S.; Vezzoli, G. The Continental Crust as a Source of Sand (Southern Alps cross-section, Northern Italy). *J. Geol.* **2006**, *114*, 533–554. [[CrossRef](#)]
132. Garzanti, E.; Vezzoli, G.; Andò, S. Paleogeographic and paleodrainage changes during Pleistocene glaciations (Po Plain, Northern Italy). *Earth Sci. Rev.* **2011**, *105*, 25–48. [[CrossRef](#)]
133. Weltje, G.J. End-member modelling of compositional data: Numerical statistical algorithms for solving the explicit mixing problem. *Math. Geol.* **1997**, *29*, 503–549. [[CrossRef](#)]
134. Garzanti, E.; Resentini, A.; Vezzoli, G.; Andò, S.; Malusà, M.; Padoan, M. Forward compositional modelling of Alpine orogenic sediments. *Sediment. Geol.* **2012**, *280*, 149–164. [[CrossRef](#)]
135. Cervený, P.F.; Johnson, N.M.; Tahirkheli, R.A.K.; Bonis, N.R. Tectonic and geomorphic implications of Siwalik group heavy minerals, Potwar plateau, Pakistan. In *Tectonics of the Western Himalayas; Special Papers 232*; Malinconico, L.L., Lillie, R.J., Eds.; Geological Society of America: Boulder, CO, USA, 1989; pp. 129–136.
136. Yamamoto, H. Contrasting metamorphic P-T-time paths of the Kohistan granulites and tectonics of the western Himalayas. *J. Geol. Soc.* **1993**, *150*, 843–856. [[CrossRef](#)]
137. Jagoutz, O.; Schmidt, M.W. The formation and bulk composition of modern juvenile continental crust: The Kohistan arc. *Chem. Geol.* **2012**, *298*, 79–96. [[CrossRef](#)]

138. Keane, S.D.; Morrison, J. Distinguishing magmatic from subsolidus epidote: Laser probe oxygen isotope compositions. *Contrib. Mineral. Petrol.* **1997**, *126*, 265–274. [[CrossRef](#)]
139. Spiegel, C.; Siebel, W.; Frisch, W.; Berner, Z. Nd and Sr isotopic ratios and trace element geochemistry of epidote from the Swiss Molasse Basin as provenance indicators: Implications for the reconstruction of the exhumation history of the Central Alps. *Chem. Geol.* **2002**, *189*, 231–250. [[CrossRef](#)]



© 2019 by the authors. Licensee MDPI, Basel, Switzerland. This article is an open access article distributed under the terms and conditions of the Creative Commons Attribution (CC BY) license (<http://creativecommons.org/licenses/by/4.0/>).